PREREDUCTION AND MAGNETIC SEPARATION OF LOW GRADE MANGANESE ORE

by

Yubo Gao

A thesis submitted to the faculty of
The University of Utah
in partial fulfillment of the requirements for the degree of

Master of Science

Department of Metallurgical Engineering

University of Utah

August 2011

The University of Utah Graduate School

STATEMENT OF THESIS APPROVAL

The thesis of **Yubo Gao**

has been approved by the following supervisory committee members:

Hong Yong Sohn	, Chair	**April 29, 2011** Date Approved
Hang Goo Kim	, Member	**April 29, 2011** Date Approved
Zhigang Zak Fang	, Member	**April 29, 2011** Date Approved

and by **Jan D. Miller**, Chair of the Department of **Metallurgical Engineering**

and by Charles A. Wight, Dean of The Graduate School.

ABSTRACT

Because of intensive mining of high-grade manganese ores for a long time while leaving behind the low-grade ores, the utilization of the latter has become necessary. There are several physicochemical differences among the components in manganese ores, which can be used for the enrichment of manganese. In particular, the abundant low-grade manganese ores, which contain iron oxide, may be upgraded by prereduction and magnetic separation.

In this study, ferruginous low-grade manganese ore was prereduced by CO, which converted iron oxide to Fe_3O_4 while manganese oxide was reduced to MnO. Then, the iron-rich component was collected by magnetic separation. The effects of sample particle size and various other reduction parameters on the efficiency of magnetic separation were studied. Under the optimum experimental conditions, the manganese content in the ore increased from around 36% to more than 45%, and almost 50% of iron were removed at a Mn loss of around 5% by this method.

For the kinetics study of the reduction of Mn_3O_4 in the ore, TGA was used to investigate the reduction extent and reduction rate at different reduction conditions. During the reduction, the changes in the phases were examined by XRD. Based on the experimental data as well as the physical features of sample particles used in this work, the nucleation and growth equation was determined to best represent the reduction rate

and a complete rate equation was formulated. In addition, the effects of such major impurities as Fe_2O_3 and SiO_2 on the reduction process were also determined in this work.

CONTENTS

LIST OF TABLES

LIST OF FIGURES

ACKNOWLEDGMENTS

First of all, I would like to express my gratitude to my supervisor, Professor H.Y. Sohn, for his seasoned instructions and valuable advice on this research project, and also for his helpful classes.

Besides my advisor, I would like to thank the rest of my thesis committee members: Dr. Hang Goo Kim and Professor Zak. Z. Fang for their help, suggestions, and kind concern on my study and research work.

I also want to extend my thanks to all of the faculty, staff and students, who supported me in many ways during the completion of the project.

This project is supported by Research Institute of Industrial Science and Technology (RIST), Pohang, Korea. My gratitude also goes to POSCO Co. for supplying the manganese ores and for chemical analysis of sample manganese ores.

Lastly, I owe my deepest gratitude to my beloved family, especially my parents. Without their continuous encouragement and moral support, I would not have finished this thesis.

CHAPTER 1

INTRODUCTION

1.1 Background

1.1.1 Mineralogy and reserve of manganese ore

At about 0.12%, manganese is the twelfth most abundant element in igneous rocks contained in the earth's crust. This concentration is quite modest compared with alumina at 15.4%, iron at 6.9%, and even titanium 1.1%, but considerably higher than what are regarded as common commercial metals like copper at 0.01%, zinc at 0.004%, and lead at 0.002%. [1]

Manganese does not occur in an elemental state in nature. For the most part, manganese tends to replace two sets of elements—firstly the alkaline earths: calcium, barium, and magnesium, and secondly aluminum and iron. Being transported and concentrated in a variety of geologic environments, manganese is present in innumerable minerals, some 250 of which may be classified as "manganese minerals". The most important minerals may be divided into oxides, carbonates, silicates, and others. Hydrated and anhydrous oxides are by far the most common and varied manganese ores, followed by the far rarer carbonate and silicate. [2]

According to the publication of US Geological Survey in 2004, [3] as shown in Table 1-1, South Africa accounts for more than 80% of the world's identified manganese resources, and Ukraine accounts for about 10% more.

Table 1-1 Manganese: reserves and reserve base (million tones, Mn content)

Country	Reserves	Reserve base
Australia	32,000	82,000
Brazil	23,000	51,000
China	40,000	100,000
Gabon	20,000	160,000
India	15,000	33,000
Mexico	4,000	9,000
South Africa	32,000	4,000,000
Ukraine	140,000	520,000
Other countries	small	small
World total (rounded)	300,000	5,000,000

1.1.2 Grades and classification of manganese ore

The normal classification of manganese ore, is as follows: [4]

- Manganese ores, containing more than 35% Mn suitable for the manufacture of high-ore low-grade ferromanganese;
- Ferruginous manganese ores containing 5 ~ 35% Mn suitable for the manufacture of spiegeleisen;
- Manganiferous iron ores with 5 ~ 10% Mn used for the manufacture of manganiferous pig iron.

In practice, manganese ores and concentrates have a wide and complex range of chemical and physical specifications most often employing a specific end-use prefix: [5]

Metallurgical-grade used in the iron and steel industry requires 35 ~ 55% Mn, generally with a Mn/Fe ratio larger than 5.

Battery-grade requires 70 ~ 85% MnO_2, that is equivalent to 44 ~ 54% Mn, and should contain less than 0.05% of metals more electronegative than zinc, such as copper, nickel, cobalt, and arsenic.

Chemical-grade has various specifications depending on the specific end use such as feedstock for electrolytic manganese and manganese dioxide, manganese chemicals, colorants, and uranium processing.

Fertilizer and feed grade requires 30 ~ 60% Mn; ferrites need particularly low levels of CaO, K_2O, Na_2O, BaO, and SiO_2.

Besides, manganese ores can also be classified by grades as shown in Table 1-2.

1.1.3 Metallurgical uses of manganese ore

Manganese markets are dominated by metallurgical uses, in particular the production of ferroalloys and the subsequent use in steelmaking. Figure 1-1 illustrates how products of manganese ore are used in metallurgy.

Figure 1-1 indicates that very minor quantities of manganese ore are used directly or at the other extreme converted to manganese metal, and the bulk of the manganese ore consumed in steelmaking is converted to ferromanganese.

Table 1-2 Classification of manganese ore by grades [5]

Mn ore	High Grade	Medium grade	Low Grade	Steel Mill Grade
% Mn	> 44	40 - 44	35 - 40	28 - 35

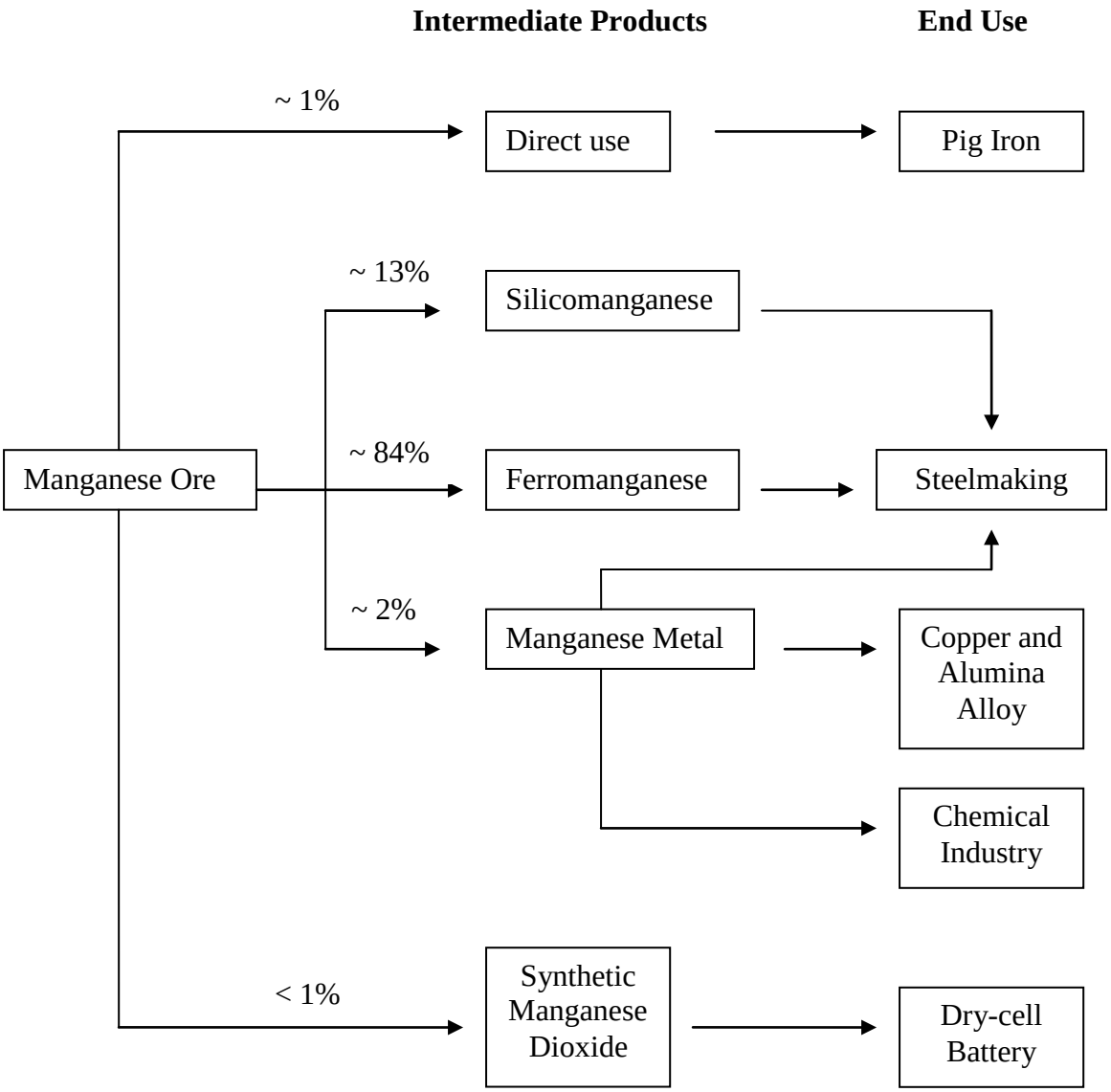

Figure 1-1 The production and consumption of intermediate manganese products (adapted from [6])

1.1.4 Application and production of ferromanganese alloy

Ferromanganese, either as a high-, medium-, or low-carbon grade, is principally used as a deoxidizer in steelmaking or as a manganese source in the manufacture of high-manganese steel.

The production of ferromanganese from manganese ore can be carried out in either a blast furnace or an electric submerged-arc furnace. Although the choice is based on a number of economic factors, electric furnaces tend to be less capital intensive, and are more flexible in that they can handle a wider range of ore composition and size. Even though the electric furnaces do not require blast-furnace quality coke, they do depend on electrical energy. To improve the economics of the process, it is desired to reduce the power consumption of the electric furnace as much as possible. One of the possible methods of achieving this is to arrange prereduction of the ore outside the electric furnace by the use of a cheaper reductant.

1.1.5 Prereduction of manganese ore

Prereduction can be considered as a thermal beneficiation step, which improves the grade of ore, depending on intensity of reduction and quality of raw materials.

In addition, when manganese ores containing iron oxides are subjected to prereduction, the higher iron oxide minerals also get reduced to lower oxide form and are amenable to removal by magnetic separation.

These in turn engender such benefits as savings in transportation costs, and utilization of lean grade ores and the outgoing gases from the furnace as well as decreased power consumption in the following smelting process. It was reported that the energy consumption dropped from about 3000 kWh/ton FeMn to about 1600 kWh/ton

FeMn when prereduced ore was used instead of naturally occurring ore in the electric furnace. [7]

Therefore, naturally occurring manganese ores generally need to be first subjected to prereduction, and it is of practical interest especially for the utilization of low grade manganese ores.

1.2 Previous study on the prereduction of manganese ore

For the prereduction of manganese ore, the carbothermic reduction has been investigated from various points of view.

Ostrovski and Webb [8] investigated the reduction mechanism of a siliceous manganese ore by graphite and found there were two stages of reduction. In the first stage, iron oxide was reduced to iron and manganese oxide to MnO by CO. During the second stage, MnO was reduced to Mn by carbon dissolved in the metallic phase. In comparison with the two-stage mechanism, Eric and Burucu [9] observed in their study, in which Mamatwan manganese ore was reduced by powder graphite under argon atmosphere between 1000 and 1350˚C, the reduction went through three stages. During the first stage, higher manganese and iron oxides were reduced to MnO and FeO, respectively. In the second stage, metallic nuclei rich in iron were formed as randomly distributed small globules. The third stage was the reduction of remaining MnO and FeO by carbon dissolved in the carbide phase.

Hansen et al. [10] studied the reducibility of three different manganese ores (siliceous, carbonate, oxide) with coke, and found that they reacted differently upon heating. Samples that were essentially manganese oxides readily reacted to form the lower oxides at lower temperature (700 ~ 800˚C). The ores that were primarily

carbonates reduced to the divalent oxides at higher temperature (1150 ~ 1200˚C). Manganese silicate ores were least amenable to reduction.

The extent and kinetics of manganese ore reduction also strongly depend on the ore composition. It is reported by Yastreboff [11] that silica has a strong retarding effect on the carbothermic reduction of manganese ore. This is in a good agreement with the result obtained by Rankin, [12] who also found that the addition of Fe_2O_3 increased the rate of reduction, and the effects of CaO, MgO, and Al_2O_3 were very small, while there was a marked increase in reduction rate when K_2CO_3 and Na_2CO_3 were present. Besides, Antonov and Chufarov [13] reported that additions of Fe_2O_3 and K_2CO_3 accelerated the reduction of manganese ore.

Dewar and See [14] investigated the influence of different carbonaceous reducing agents on the rate of reduction of Mamatwan manganese ore in the temperature range 850 to 1500˚C under neutral atmosphere. Although there was no big difference in the mode of reduction with different reducing agents, both the extent and rate of reduction were enhanced when the reactivity of reducing agents toward CO_2 increased. At the same time, it is evidently shown in the study conducted by Kor [15] that the reduction rate of manganese oxides by coconut char is much faster than that of pure graphite at temperature between 900 and 1200˚C.

The effect of atmosphere on the carbothermic reduction of manganese oxide and manganese ore were studied by several researchers. Kononov R. and Ostrovski O. [16] studied the carbothermic reduction of manganese oxides in hydrogen, helium, and argon at different temperatures. It was found that the reduction rate of manganese oxide in hydrogen was higher than in helium, and in helium higher than in argon. Ding W. [20]

examined the effect of the partial pressure of CO on the manganese ore reduction by carbon. He stated that lowering the CO partial pressure enhanced the rate of carbothermic reduction of manganese ore. Similar results were obtained by Skjervheim [21] and Yastreboff. [22] In addition, Nathaniel et al. [23] conducted the reduction of manganese ore in a gas containing methane in the temperature range 1000 ~ 1200˚C. This study found that the rate of reduction increased with increase in the level of CH_4 in the gas.

The investigations discussed above employed solid carbon as the reducing agent in almost all cases. In comparison with solid carbon, the reduction of manganese ore by CO may result in a faster rate even in a lower temperature, owing to the advantages of gaseous reduction over carbothermic reduction. [20] Up to now, however, very little research has been carried out for the gaseous reduction of manganese ore by CO, and more intensive studies on prereduction by CO are essential to develop the effective and suitable techniques for the beneficiation of ferruginous low-grade manganese ores.

1.3 Research objectives

This study concentrated on the prereduction of ferruginous low-grade manganese ore by CO followed by magnetic separation.

For the upgrading of ferruginous low-grade manganese ore by prereduction and magnetic separation, operating conditions should be controlled to reduce Fe_2O_3 to either Fe_3O_4 or metallic Fe, but not FeO, so that the iron contained in the manganese ore could be removed by magnetic separation. The mixture gas of carbon monoxide and carbon dioxide was used for the prereduction at the temperatures from 400 to 700˚C. The effect of particle size on the efficiency of magnetic separation was first studied, followed by

study on the significance and interactive effect of other different reduction parameters, including reduction time, temperature, CO content of reducing gas.

The degree of reduction of the higher oxides of manganese to the lowest oxide, MnO, achieved during the prereduction has a direct impact on the energy consumption for the subsequent process. Understanding the kinetics of prereduction is useful for controlling the process parameters to optimize specific power consumption and maximize the recovery of the metal. The effects of such parameters as reduction temperature, composition of reducing atmosphere, particle size of samples on the extent and rate of reduction were investigated. Besides, the influences of bed depth and major impurities were also studied in this work.

CHAPTER 2

PRELIMINARY STUDY AND TEST FOR PREREDUCTION OF MANGANESE ORE

2.1 Mineralogical study and chemical analysis of sample manganese ores

At the very beginning, there are two manganese ores involved in this work, designated “LP” and “LW”. All of them are provided by POSCO Co.

2.1.1 Chemical analysis

The chemical analyses of sample manganese ores are given in Table 2-1.

Table 2-1 shows that the manganese ores used in this study were of low manganese grade (< 40%) and low Mn/Fe ratio (< 3). For the production of ferromanganese alloy, it was reported by Kothari [21] that the Mn/Fe ratio of manganese ore should be at least 5:1. Therefore removal of iron therefrom is not only beneficial for the enrichment of manganese but also necessary for the further processing.

Table 2-1 Chemical compositions of original “LP” and “LW” manganese ores

Ore	Chemical Composition						
	T-Mn	T-Fe	SiO_2	Al_2O_3	CaO	P_2O_5	MgO
LP	36.6	12.7	11.7	4.01	0.12	0.17	0.11
LW	38.1	18.7	1.99	0.47	10.7	0.05	0.55

2.1.2 Phase identification

XRD test results of original “LP” and “LW” manganese ores are shown in Figure 2-1 and Figure 2-2, respectively.

As shown in Figure 2-1, the major phases of original “LP” ore were MnO_2 and SiO_2. In addition to the predominant phase of manganese — MnO_2, trace of the manganese contained in the “LP” ore was present as KMn_8O_{16}. The iron existed as Fe_2O_3 and FeO(OH). Besides, the phase of $Al_2Si_2O_5(OH)_4$ was also detected. For the “LW” ore, as indicated by Figure 2-2, the manganese and iron were present as Mn_2O_3 and Fe_2O_3, respectively. In addition, “LW” ore also contained a considerable amount of $CaCO_3$.

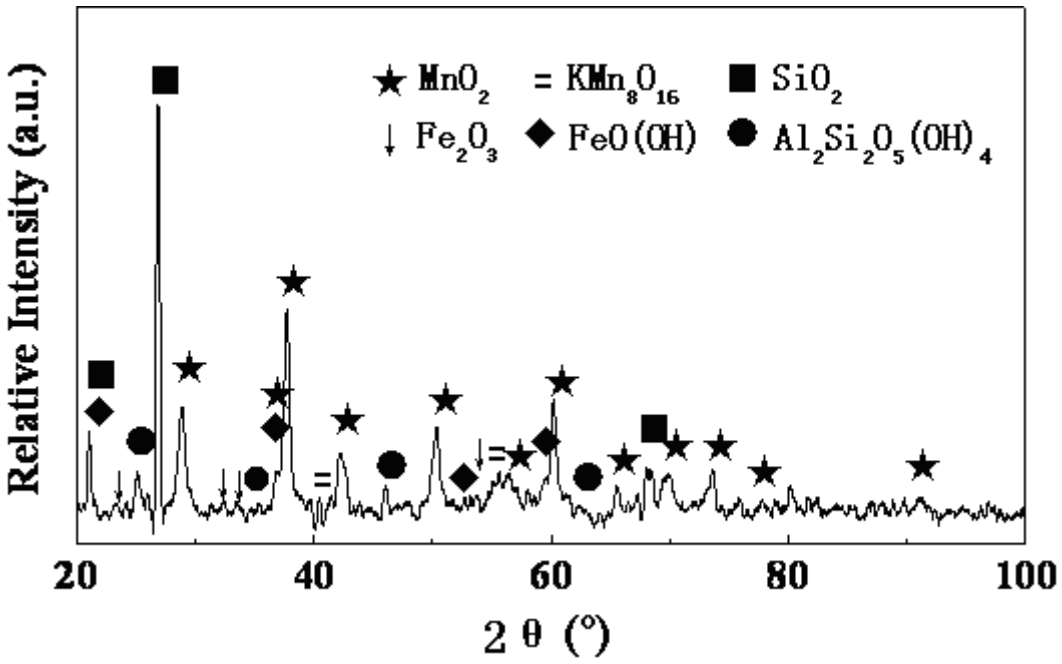

Figure 2-1 XRD pattern of original “LP” ore

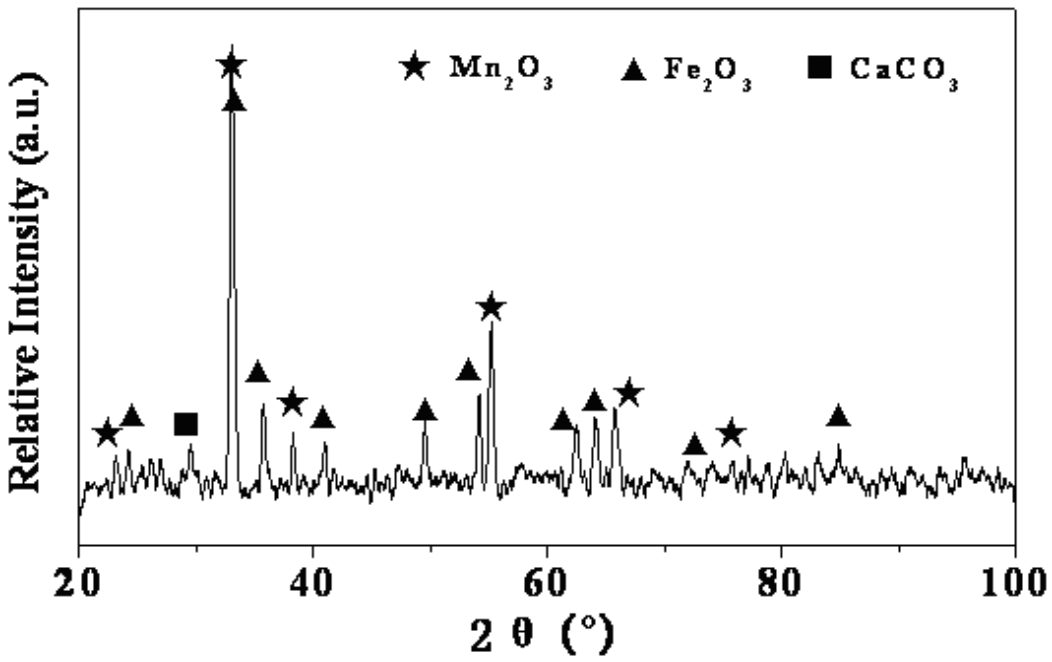

Figure 2-2 XRD pattern of original “LW” ore

2.2 Thermal decomposition behavior study of sample manganese ores

As shown in Figures 2-1 and 2-2, there were some impurity phases contained in the original sample ores. In order to improve the Mn content, it is necessary to reduce the amount of these impurities. One of the methods used to achieve this is calcination, during which volatile components and moisture can be removed, and hydrates and carbonates contained in the ore are decomposed. Moreover, during the reduction, the weight loss due to the reduction of manganese and iron oxides may be masked by weight loss due to thermal decomposition of these impurities and removal of water, existing in ores in the forms of moisture and chemical combined water. Therefore, as far as the kinetics study of reduction is concerned, calcination is also recommended in order to make the weight loss in the reduction to be totally attributable to the reduction of manganese and iron oxides. Investigation on thermal decomposition behavior is prerequisite to determine the calcination temperature.

Thermal decomposition experiments were conducted by using a continuously recording electro-balance (Cahn, RTL #7000 for 110v 60Hz, Cahn Instruments, California, USA) under argon atmosphere. Samples were heated up to 1000˚C, and the nonisothermal weight loss curves as well as the temperature profile are given in Figure 2-3, which shows that the "LP" ore begins to lose weight at a relatively lower temperature, and also achieves a larger weight loss, compared with "LW" ore. This resulted from the difference in chemical phases. For "LP" ore, the weight loss is mainly due to the thermal decomposition of MnO_2, FeO(OH) and $Al_2Si_2O_5(OH)_4$, while the weight loss of "LW" ore mostly resulted from the thermal decomposition of Mn_2O_3 and $CaCO_3$, all of which require a higher decomposition temperature. In addition, Figure 2-3 also indicates that, when temperature increases to 900˚C, the weight of "LP" ore does not change distinctly any more, and the corresponding temperature for "LW" ore is 950˚C.

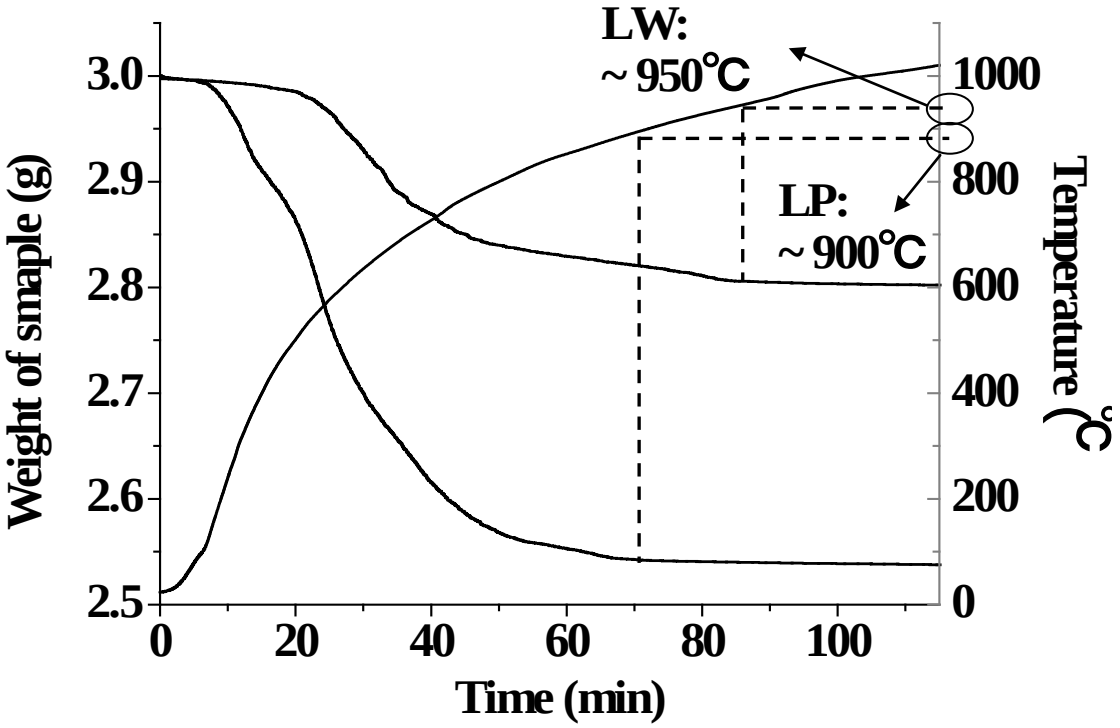

Figure 2-3 Test results of thermal decomposition behavior test

2.3 Magnetic properties of MnO-rich and Mn_3O_4-rich ores

Besides the removal of volatile components and decomposition of hydrates and carbonates, manganese oxides contained in the original ores also underwent thermal decomposition during the calcination. According to the equilibrium diagram of Mn-O system, manganese oxides contained in the original ore should be converted to Mn_3O_4 below the calcination temperature less than 1000˚C, which was verified by the XRD test result of calcinated ores, as shown in Figures 2-4 and 2-5.

Besides thermal decomposition, manganese oxides may further be reduced to MnO in the subsequent reduction. In order to find a phase of Mn that prompts magnetic separation, a simple test was conducted using a magnet to evaluate the magnetic characteristics of Mn_3O_4-rich particle (darker, top) and MnO-rich particle (lighter, bottom), as shown in Figure 2-6.

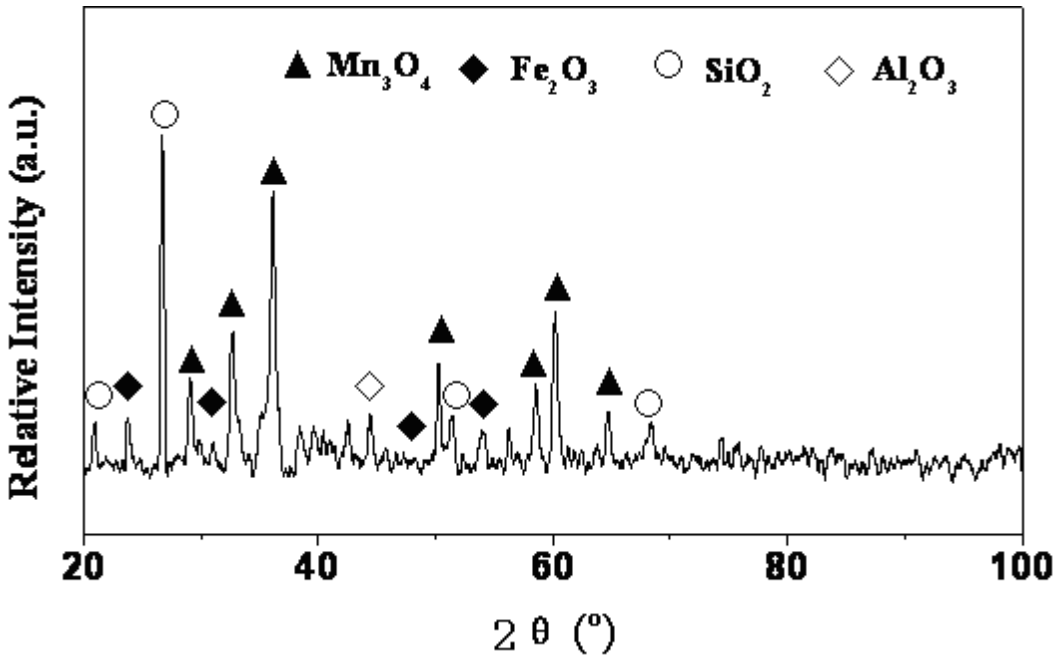

Figure 2-4 XRD pattern of calcinated “LP” ore

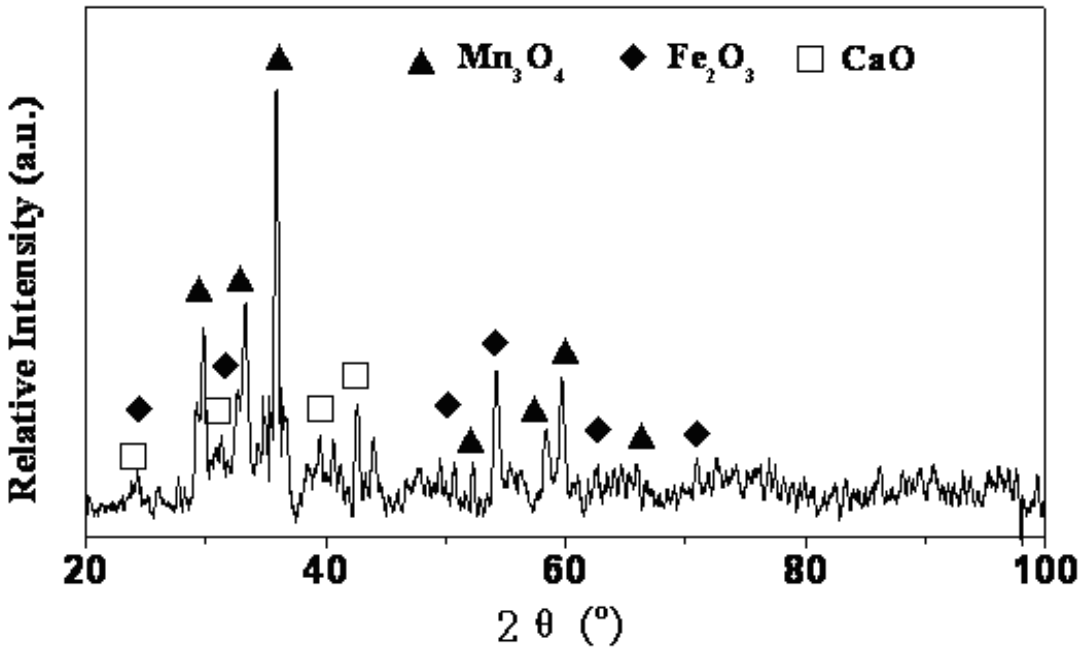

Figure 2-5 XRD pattern of calcinated “LW” ore

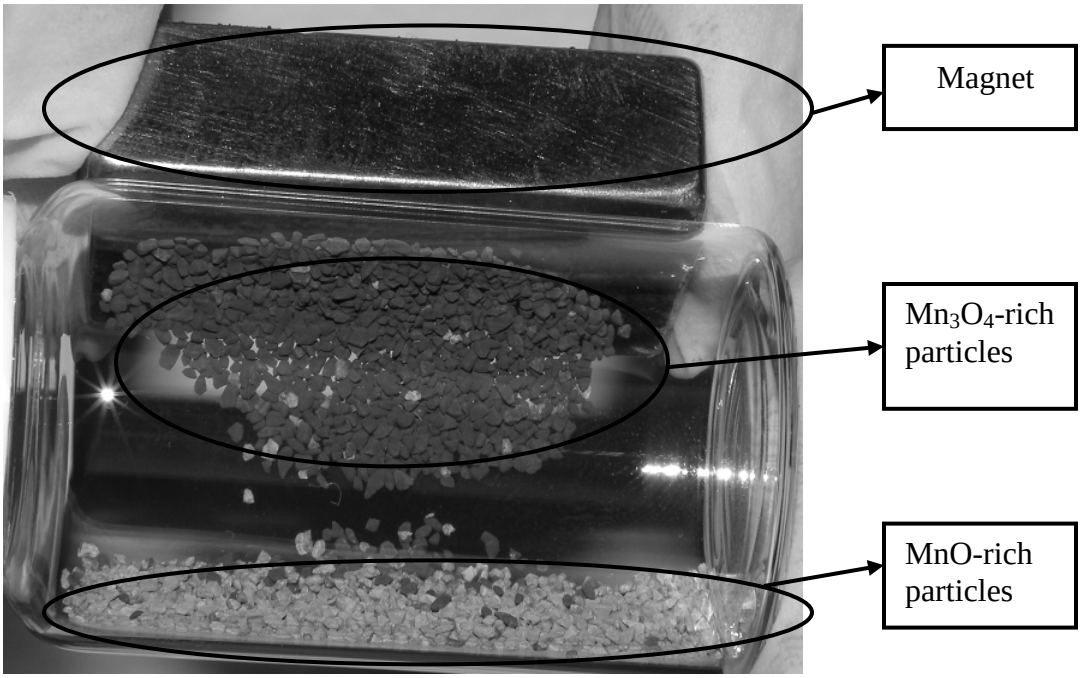

Figure 2-6 Magnetic test result for Mn_3O_4-rich and MnO-rich particles

The test results show that, while the MnO predominant particle (light grey) is nonmagnetic or weakly magnetic, the Mn_3O_4 predominant particle (dark grey) is strongly magnetic. This is in good agreement with the result obtained by other researchers, [22, 23] who also found that Mn_3O_4-rich manganese ore displayed a strong ferromagnetic behavior at room temperature.

As a result, in order to remove iron from manganese ore by magnetic separation, the Mn_3O_4 in calcinated manganese ore should be further converted to MnO. Otherwise, the manganese in the form of Mn_3O_4 will also be removed by magnetic separation, thus resulting in a severe loss of manganese.

2.4 Thermodynamics of prereduction

When manganese ores containing iron oxides are subjected to prereduction, it is not thermodynamically possible to reduce manganese oxides to go beyond MnO by C or CO at temperatures from 400 to 1000°C, while the iron oxide can be reduced to Fe_3O_4 and metallic Fe. The latter two are strongly magnetic and thus amenable to removal by magnetic separation.

In this study, prereduction of ferruginous low-grade manganese ore was conducted by using a gas mixture of CO and CO_2. While manganese oxide was converted to MnO, which is not attracted by magnet, iron oxide was selectively reduced only to Fe_3O_4, because of its stronger magnetism and lower requirements both in power consumption and reduction gas compared with those for reducing it to metallic Fe. The selectivity of reduction was achieved by controlling the reduction conditions at the overlapped stable region of MnO and Fe_3O_4 in the corresponding equilibrium diagram, shown in Figure 2-7.

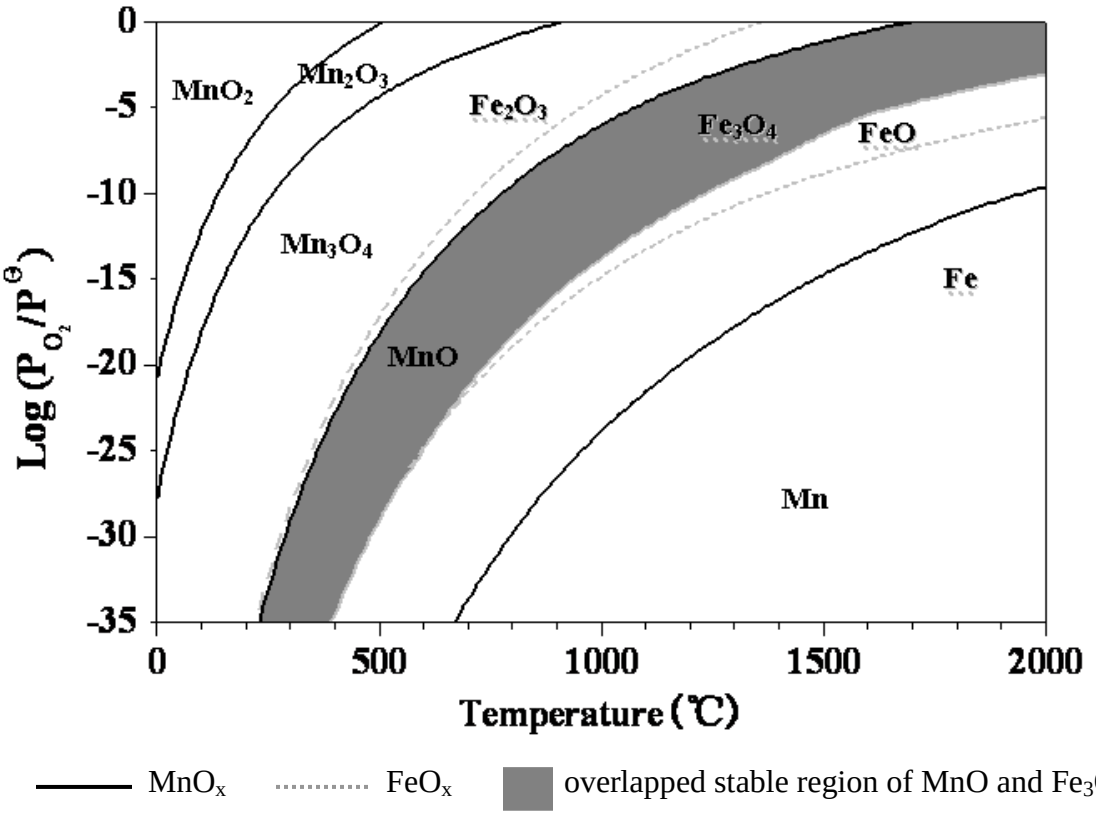

Figure 2-7 Temperature—oxygen potential diagram for Mn-Fe-O system

2.5 Preliminary test for magnetic separation

Preliminary tests were firstly undertaken to study the feasibility of magnetic separation for prereduced sample ores.

2.5.1 Preliminary test of "LP" ore

In the preliminary test, the milled "LP" sample particles, in the size range of 500 ~ 1000 μm, were firstly calcinated at 900˚C for 3 hours in argon atmosphere. The subsequent prereduction was conducted at 600˚C for 5 hours, using a mixture gas of CO and CO_2 (CO/CO_2:30/70). The reduced samples were reground gently so as to break up the loosely fused particles.

As expected, magnetic separation was achieved for prereduced “LP” particles, and the XRD patterns of magnetic and nonmagnetic parts are shown in Figure 2-8 and Figure 2-9, respectively.

Figures 2-8 and 2-9 indicate that, while the magnetic part mainly consists of Fe_3O_4 and MnO, the major phases contained in the nonmagnetic part are MnO, SiO_2, and Al_2O_3. Therefore, iron was effectively concentrated to the magnetic part. At the same time, a certain amount of MnO is also detected in the magnetic part by XRD, although it is not magnetic. This is probably due to the similar physicochemical properties of iron and manganese, rendering to a close attachment of iron compounds and manganese compounds. As a result, MnO accompanied with Fe_3O_4-rich particles may also be introduced to magnetic part during the magnetic separation.

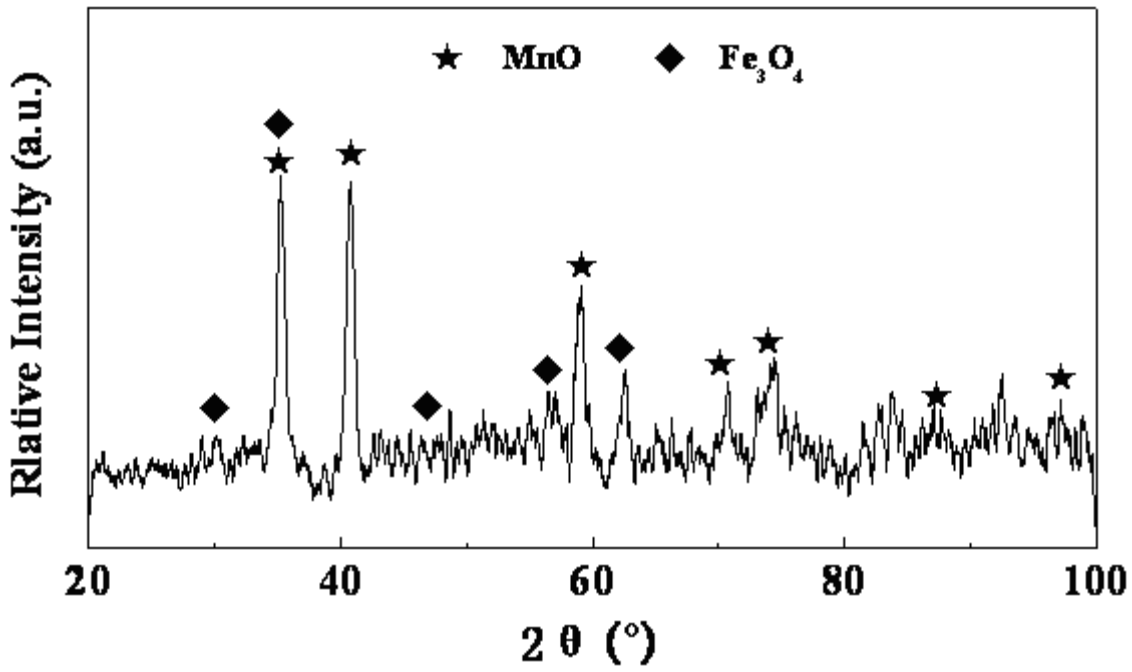

Figure 2-8 XRD pattern of magnetic part of preliminary test for “LP” ore

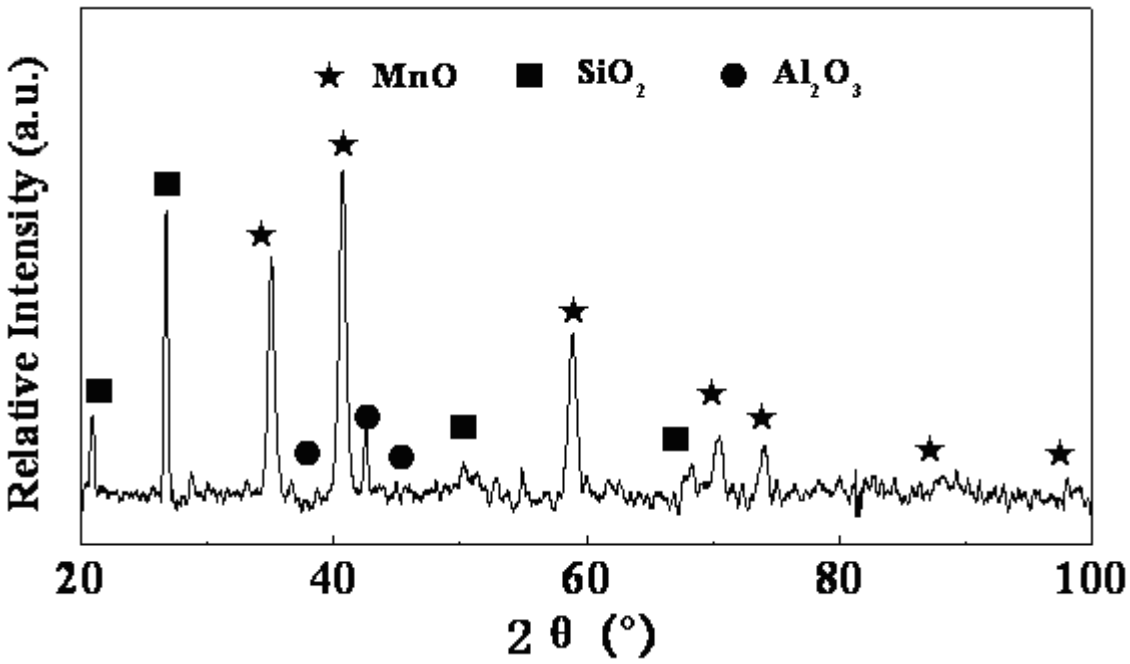

Figure 2-9 XRD pattern of nonmagnetic part of preliminary test for “LP” ore

2.5.2 Preliminary test of “LW” ore

The “LW” sample particles within particle size range of 500 ~ 1000 μm obtained after ball milling and sieving were used for the preliminary test. Sample particles were firstly calcinated at 950˚C in argon, followed by reducing at 600˚C by a gas mixture of CO and CO_2 (CO/CO_2 : 30/70) for 5 hours. However, during the subsequent magnetic separation, the major part of the reduced “LW” sample particle is magnetic, and even further grinding has very limited impact on the efficiency of magnetic separation. As a result, effective removal of iron from reduced “LW” manganese ore by magnetic separation was not achieved.

2.5.3 Iron distribution analysis

As demonstrated by the previous tests, while prereduction enabled an effective removal of iron from “LP” ore by magnetic separation, the effective magnetic separation

for the removal of Fe from reduced “LW” ore was not achieved, even after further grinding into finer particles. In order to find out the reason for this fact, the distribution of Fe both in the original “LP” and “LW” ores was tested by EDAX, and the test results of element analysis for iron are summarized in Figures 2-10 and 2-11.

As shown in Figure 2-10, for the “LP” sample particles, the iron content varies with different areas. Evidently, iron-rich area and iron-poor area are presented in “LP” sample particles. In the case of “LW” sample particles, Figure 2-11 indicates that iron is distributed uniformly, and the iron contents of different “LW” particles also roughly consist with each other. Thus, without considering other impurity components, the effect of iron distribution on efficiency of magnetic separation, used for upgrading of “LP” and “LW” ores, could be schematically demonstrated by Figure 2-12.

As demonstrated by Figures 2-12 (a) and (b), the difference in the effectiveness of iron removal by magnetic separation for “LP” and “LW” manganese ores likely resulted from the difference in iron distribution.

On the basis of preliminary test results and the related analysis, ”LP” ore was selected as the target sample for the subsequent study.

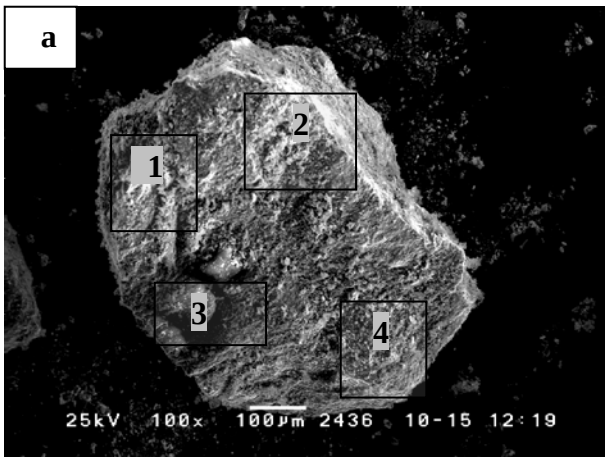

Area	Fe content (wt%)
1	1.9
2	1.5
3	5.1
4	0.5

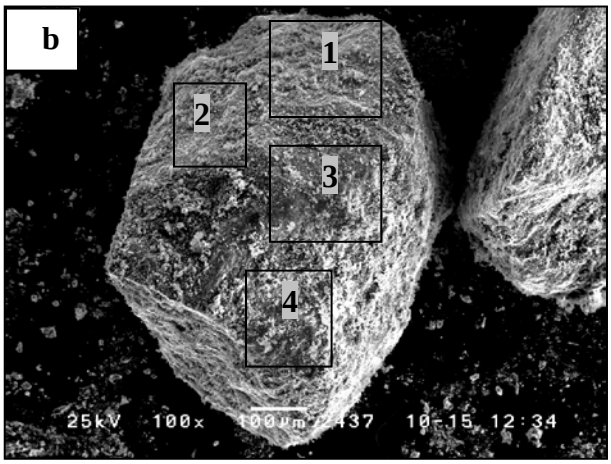

Area	Fe content (wt%)
1	2.9
2	4.7
3	17.3
4	24.4

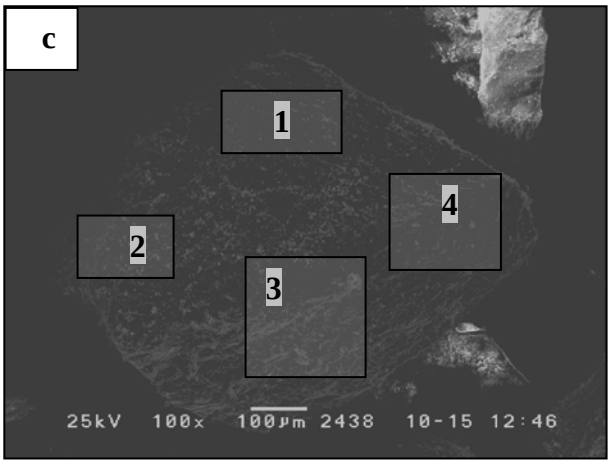

Area	Fe content (wt%)
1	4.8
2	11.7
3	2.9
4	3.5

Figure 2-10 Iron distribution in original “LP” sample particles

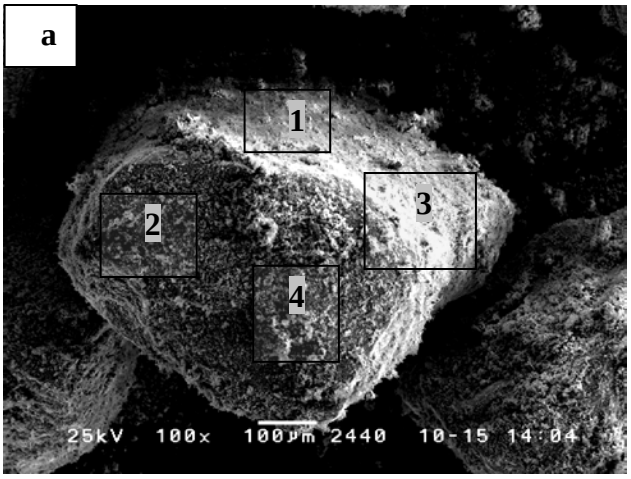

Area	Fe content (wt%)
1	18.2
2	19.2
3	22.9
4	22.9

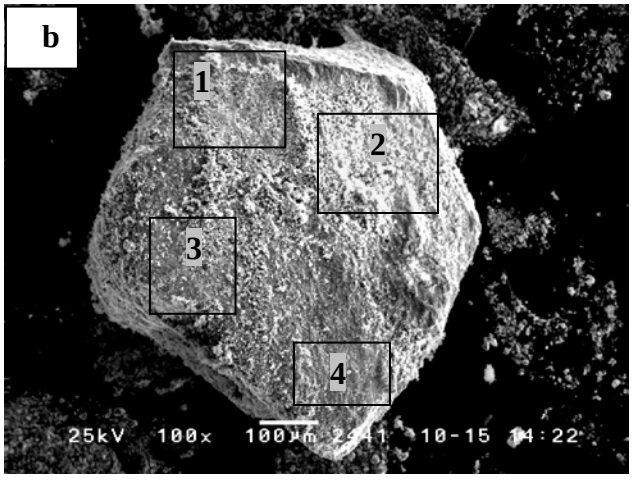

Area	Fe content (wt%)
1	22.6
2	23.4
3	23.9
4	24.1

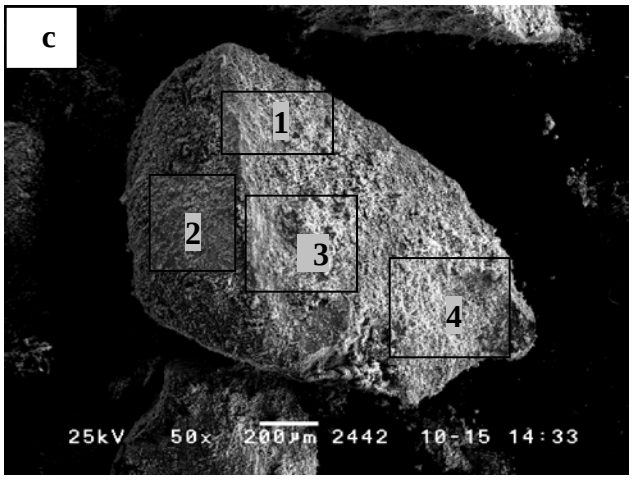

Area	Fe content (wt%)
1	22.3
2	18.6
3	18.5
4	19.2

Figure 2-11 Iron distribution in original “LW” sample particles

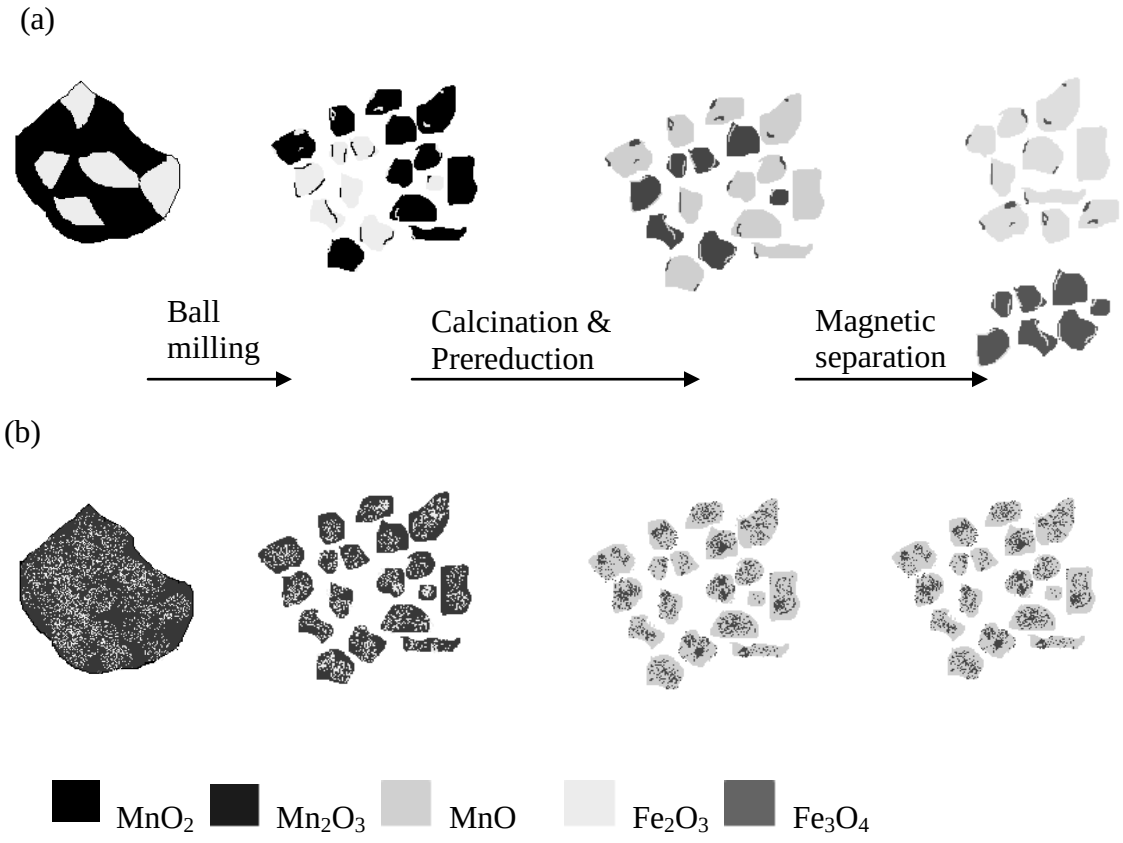

Figure 2-12 Schematic diagram for the effect of iron distribution on magnetic separation: (a) “LP” ore, (b) “LW” ore.

CHAPTER 3

UPGRADING OF MANGANESE ORE BY PREREDUCTION AND MAGNETIC SEPARATION

3.1 Experimental

3.1.1 Sample preparation

The original "LP" ore used in this study were milled and sieved. The most frequently used size of sample particles was less than 105 μm. However, several different size fractions were also prepared so that the effect of particle size on the magnetic separation could be investigated. Prior to reduction experiments, the milled sample particles were calcinated at 900˚C for 3 hours in argon, so as to remove the volatile component and to decompose the hydrates and carbonates contained in the original ore.

3.1.2 Procedure and apparatus

In this study, the prereduction of calcinated "LP" ore was conducted by using a gas mixture of CO and CO_2 as the reducing agent in the temperature range of 400 ~ 700˚C. The total gas flow rate was maintained at 1.5 NL/min. The reduced sample particles were gently reground, followed by magnetic separation. The magnetic separation was simply conducted with a magnet, whose magnetic strength was 870 Gauss. The Mn and Fe contents of various reduced and separated samples were analyzed by inductively coupled plasma (ICP).

The reduction experiments were carried out by using a horizontal high-temperature resistance furnace with a stainless steel tube (internal diameter: 40 mm, outside diameter: 55 mm, length: 1200 mm). The temperature of the furnace was controlled by a Lindberg temperature controller (model: 59545, series No.:800067), and the temperature of sample was measured by a K-type thermocouple. The schematic diagram of experimental apparatus is illustrated in Figure 3-1.

3.1.3 Method

In this study, the effect of particle size was first studied, followed by three sets of single-factor experiments so as to investigate the effects of such reduction parameters as reduction time, temperature, and CO content. Based on the test results of single-factor experiments, a two-level full factorial design was further used to investigate the significance and interactive effects of different reduction parameters.

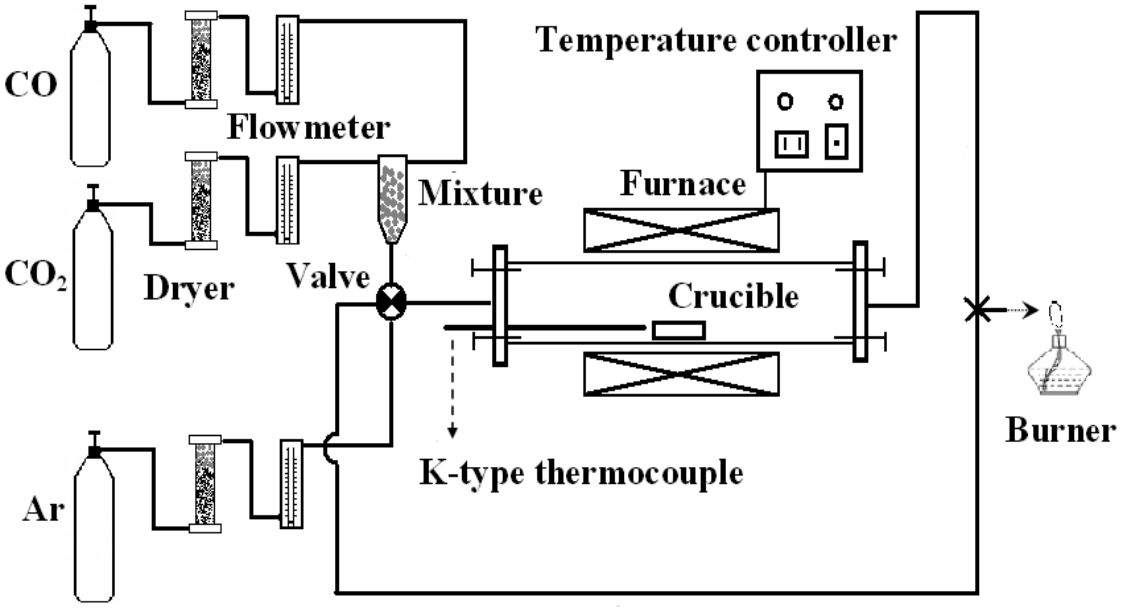

Figure 3-1 Schematic diagram of experimental apparatus

3.2 Results and discussion

As discussed below in section 3.2.5, the base-level experiments showed a good reproducibility of the experiments.

3.2.1 The effect of particle size

To investigate the effect of particle size on the efficiency of magnetic separation, the reduction was conducted for 5 hours under the gas atmosphere of CO/CO_2: 30/70 at 600˚C.

The ICP test result for various reduced and separated samples within different particle size ranges is summarized in Table 3-1, the corresponding weight percent of magnetic part and that of nonmagnetic part for each particle size range are also listed in the Table 3-1.

Table 3-1 ICP test result for various reduced samples after magnetic separation

Particle size (μm)	Magnetic part			Nonmagnetic part		
	Wt% relative to reduced sample	ICP		Wt% relative to reduced sample	ICP	
		Content of Fe (Wt%)	Content of Mn (Wt%)		Content of Fe (Wt%)	Content of Mn (Wt%)
500 ~ 1000	3.3	24.7	33.7	96.7	3.5	42.1
210 ~ 297	4.2	23.6	38.7	95.8	3.8	40.1
105 ~ 150	6.2	26.9	29.7	93.8	3.1	44.2
74 ~ 105	7.5	29.8	28.7	92.5	2.9	45.6
62 ~ 74	7.8	31.4	29.1	92.2	2.7	45.4
< 45	7.5	31.8	29.1	92.5	2.7	43.3

Based on the ICP analysis of Mn and Fe contents of various reduced and separated samples, as well as the weight percent of magnetic part relative to overall weight of reduced sample, the effect of particle size on the magnetic separation can be further evaluated in terms of in terms of the following factors:

$$\%\ \text{Fe removed} = \frac{\text{Amount of Fe in magnetic part}}{\text{Total amount of Fe in reduced sample}} \times 100 \text{ ----------(3.1);}$$

$$\%\ \text{Mn lost} = \frac{\text{Amount of Mn in magnetic part}}{\text{Total amount of Mn in reduced sample}} \times 100 \text{ ----------(3.2);}$$

$$\text{Mn/Fe} = \frac{\text{Content of Mn in nonmagnetic part}}{\text{Content of Fe in nonmagnetic part}} \text{ ----------(3.3).}$$

The effect of particle size on magnetic separation has been present in Table 3-2.

It can be observed from the results that the amount of iron removed by magnetic separation increases with decreasing particle size, but the manganese loss also increases,

Table 3-2 Effect of particle size on the efficiency of magnetic separation

Particle size (μm)	% Fe removed	% Mn loss	Mn/Fe ratio
500 ~ 1000	19.2	2.9	11.3
210 ~ 297	21.2	4.2	10.4
105 ~ 150	36.9	4.4	14.5
74 ~ 105	45.4	5.1	15.7
62 ~ 74	49.5	5.4	16.8
< 45	48.6	5.5	15.9

and that a smaller particle size results in a higher Mn/Fe ratio after magnetic separation. In addition, Table 3-2 also indicates that, when the particle size is below 105 μm, particle size has a much smaller effect on magnetic separation. Therefore, the particle size of the sample used in the subsequent tests is no larger than 105 μm.

3.2.2 The effect of reduction time

Such reduction parameters as reduction time, temperature, and the CO content of reducing gas were further determined in this study.

The effect of reduction time was studied at 600˚C with a mixture gas of CO and CO_2 (CO/CO_2 : 30/70). The test results of various samples conducted at different reduction times are summarized in Table 3-3.

Table 3-3 shows that the weight percent of magnetic part relative to the total reduced sample deceases distinctly when the reduction time is less than 25 minutes. In virtue of the results listed in Table 3-3, the effect of reduction time is summarized in Figures 3-2 (a) ~ (c).

Table 3-3 Test results for various samples with different reduction times

Reduction time (min)	Magnetic part			Nonmagnetic part		
	Wt% relative to reduced sample	ICP		Wt% relative to reduced sample	ICP	
		Content of Fe (Wt%)	Content of Mn (Wt%)		Content of Fe (Wt%)	Content of Mn (Wt%)
100	7.7	33.5	27.6	92.3	2.8	45.3
50	7.9	32.3	28.2	92.1	2.8	45.1
25	7.8	31.7	29.6	92.2	2.8	45.4
15	6.5	31.8	30.3	93.5	3.2	45.9
5	4.9	31.3	32.7	95.1	3.4	44.3

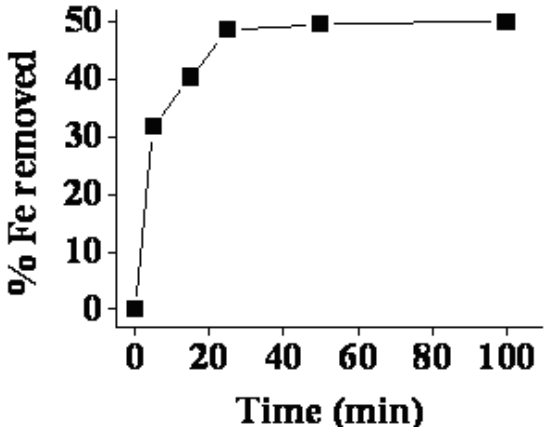

(a)

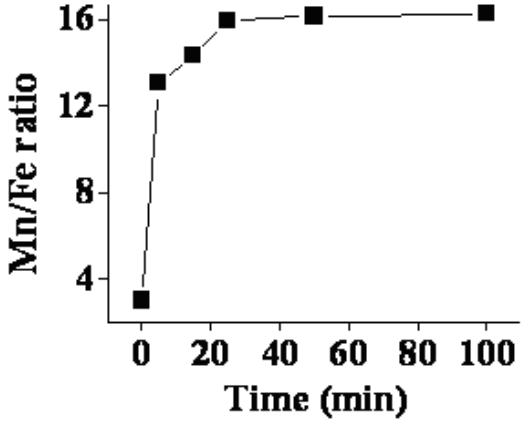

(b)

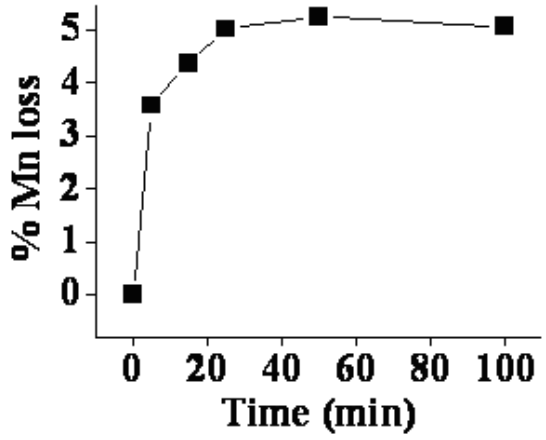

(c)

Figure 3-2 The effect of reduction time at 600˚C and 30% CO: (a) % Fe removed (b) Mn/Fe achieved by magnetic separation; (c) % Mn lost

From the above figures, it is not difficult to find that, in the reduction time range from 5 to 25 minutes, there is a remarkable increase with the increasing of roasting time in the amount of removed iron and the Mn/Fe ratio after magnetic separation. At the same time, the amount of manganese lost during the magnetic separation also increases slightly from around 3.6 to 4.9%. Further increase in the reduction time beyond 25 minutes has only a small effect on the magnetic separation.

3.2.3 The effect of temperature

The effect of temperature was investigated in the range from 400 to 700˚C. The sample particle was reduced by a CO-CO_2 mixture (CO/CO_2 = 30/70) for 25 minutes at different temperatures, followed by magnetic separation. The test results obtained for various samples reduced at different temperatures are presented in Table 3-4.

The weight percent of iron removed and that of manganese lost during magnetic separation, as well as Mn/Fe ratio achieved after magnetic separation for different reductive temperatures are shown in Figures 3-3 (a) ~ (c), respectively. It can be observed from these figures that both the weight percent of removed iron and that of manganese loss increase with increasing temperature. A higher temperature also results in a higher Mn/Fe ratio after magnetic separation. It is noted that the effect of temperature is strong below 600˚C.

Table 3-4 Test results for various samples reduced at different temperatures

Temperature (˚C)	Magnetic part			Nonmagnetic part		
	Wt% relative to reduced sample	ICP		Wt% relative to reduced sample	ICP	
		Content of Fe (Wt%)	Content of Mn (Wt%)		Content of Fe (Wt%)	Content of Mn (Wt%)
400	3.7	32.4	29.9	96.3	3.7	43.7
500	5.5	32.1	29.6	94.5	3.4	45.0
600	7.8	31.7	29.6	92.2	2.8	45.4
700	7.8	32.8	31.5	92.2	2.8	45.4

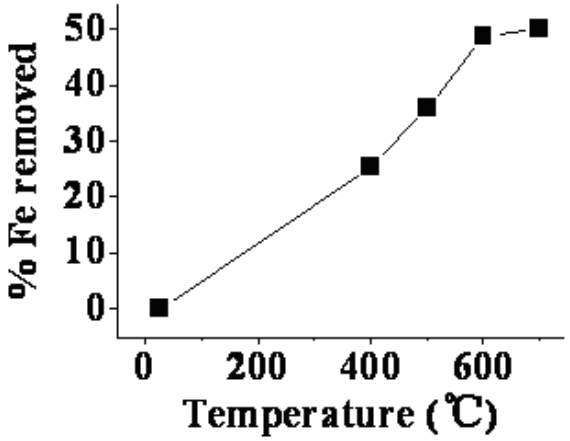

(a)

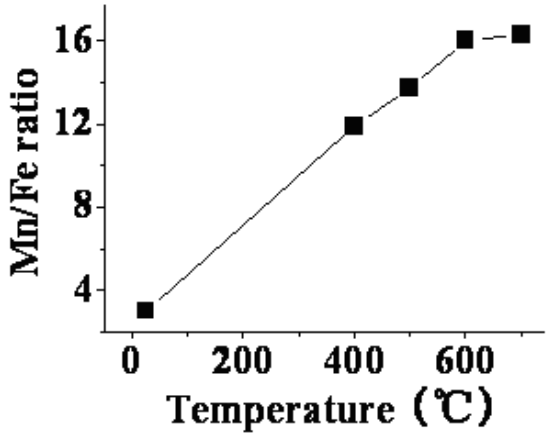

(b)

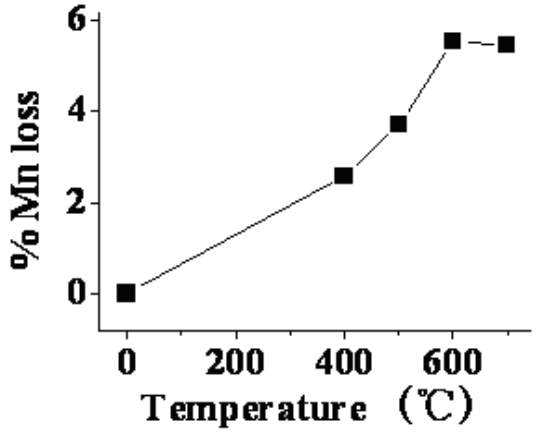

(c)

Figure 3-3 The effect of temperature with 25 min reduction time at 30% CO: (a) % of Fe removed; (b) Mn/Fe achieved by magnetic separation; (c) % of Mn lost

3.2.4 The effect of CO content of reducing gas

The effect of CO content was studied at 600˚C for 25 minutes with a gas mixture of CO and CO_2. The CO content of reducing gas was varied from 10 to 40l%. The test results for various samples reduced at different CO contents are listed in Table 3-5.

The effect of CO content on magnetic separation is demonstrated in Figures 3-4 (a) ~ (c). These figures show that a high CO content favors the removal of iron and results in a high Mn/Fe ratio after magnetic separation, especially when the CO content changes from 10 to 30 vol%. Meanwhile, the amount of manganese lost during magnetic separation also increases with increasing CO content.

Table 3-5 Test results for various samples reduced at different CO contents

Content of CO (Vol%)	Magnetic part			Nonmagnetic part		
	Wt% relative to reduced sample	ICP		Wt% relative to reduced sample	ICP	
		Content of Fe (Wt%)	Content of Mn (Wt%)		Content of Fe (Wt%)	Content of Mn (Wt%)
10	4.9	32.8	36.1	95.1	3.4	45.2
20	6.0	32.4	34.2	94.0	3.1	44.7
30	7.8	31.7	29.6	92.2	2.8	45.4
40	7.9	31.8	30.3	92.1	2.8	45.3

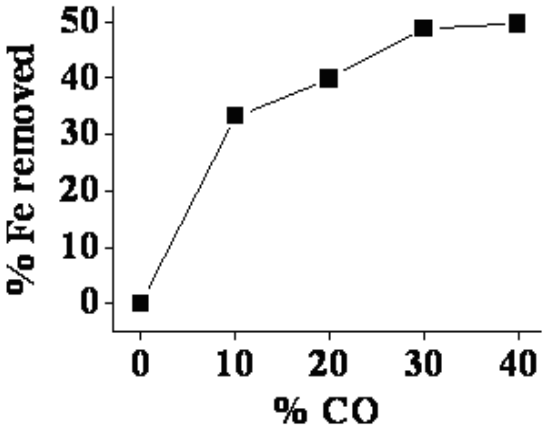

(a)

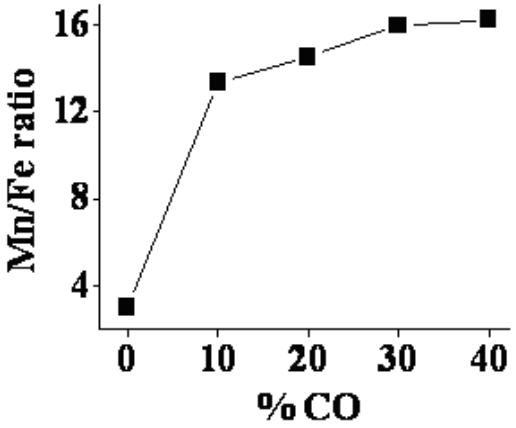

(b)

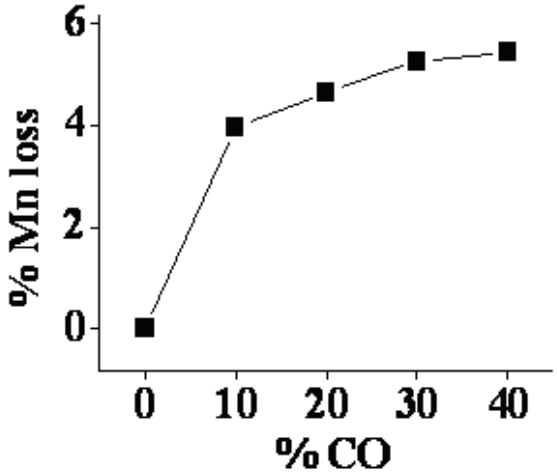

(c)

Figure 3-4 The effect of CO content at 600˚C and 25 min reduction time: (a) % of Fe removed; (b) Mn/Fe achieved by magnetic separation; (c) % of Mn lost

From the above three sets of single-factor experiments, we find that the amount of removed iron and Mn/Fe ratio in the product are improved by increasing reduction time, temperature, and CO content, with a slight increase in Mn loss. Meanwhile, the reduction condition has a smaller effect when the reduction time, temperature, and CO content increase beyond 25 minutes, 600 ˚C, and 30%. Thus, this reduction condition may be considered as the optimum condition, both regarding the efficiency of magnetic separation and cost of operation. The results of all the single-factor experiments indicate approximately linear relationships up to certain levels of experimental parameters.

3.2.5 Full factorial design for prereduction of "LP" sample

A full factorial design was used to investigate the significance and interactive effect of each experimental parameter on the magnetic separation. The parameters studied were reduction time, temperature, and CO content of reducing gas. It is envisioned that an industrial application of this upgrading process would be based on the use of CO-containing waste gases from existing operations without using large amounts of energy. Therefore, the ranges of the three parameters were decided by these considerations together with the test results of single-factor experiments, showing linear relationships within these ranges. Thus, two levels at maximum and minimum values of these variables were tested and base-level experiments were also carried out for quantitative analysis. The tested levels are listed in Table 3-6.

Table 3-6 Ranges and levels of each parameter of full factorial experiment

Parameters	Code	Lower level ($X_i = -1$)	Base level ($X_i = 0$)	Higher level ($X_i = +1$)
Time (min)	X_1	5	15	25
Temperature (˚C)	X_2	400	500	600
CO content(vol %)	X_3	10	20	30

The number of tests of this full factorial design can be calculated by the equation:

$$N = 2^{m} + k \text{ ---------- } (3.4)$$

where, N = number of tests, m = number of variables, k = number of base-level experiments. In this work, there are three variables, and three base-level experiments were carried out, as a result, 11 tests were designed and conducted. The detailed design matrix for 2^3 factorial experiments is shown in Table 3-7.

Table 3-7 Design matrix of 2^3 factorial experiments

Test	X_1	X_2	X_3	X_1X_2	X_1X_3	X_2X_3	$X_1X_2X_3$
1	1	1	1	1	1	1	1
2	1	-1	1	-1	-1	1	-1
3	-1	-1	1	1	-1	-1	1
4	-1	-1	-1	1	1	1	-1
5	-1	1	-1	-1	-1	1	1
6	1	1	-1	1	-1	-1	-1
7	-1	1	1	-1	1	-1	-1
8	1	-1	-1	-1	1	-1	1
9	0	0	0	0	0	0	0
10	0	0	0	0	0	0	0
11	0	0	0	0	0	0	0

The effects of different reduction parameters on the efficiency of magnetic separation are expressed by the following equation:

$$Y_i = a_{i0} + a_{i1}X_1 + a_{i2}X_2 + a_{i3}X_3 + a_{i12}X_1X_2 + a_{i13}X_1X_3 + a_{i23}X_2X_3 + a_{i123}X_1X_2X_3 \text{ ---------- (3.4)}$$

where, Y_1, Y_2,, Y_3 = weight percent of iron removed by magnetic separation, Mn/Fe ratio of nonmagnetic part, and weight percent of manganese lost during magnetic separation, respectively; a_i: = empirical model coefficients obtained from base-level tests; X_1, X_2,, X_3 = reduction time, temperature, and CO content, respectively.

The relationships between coded and actual values of different parameters are given as:

$$X_1 = \frac{x_1 - 15}{10} \; ; X_2 = \frac{x_2 - 500}{100} \; ; X_3 = \frac{x_3 - 20}{10} \text{ ---------- (3.6), (3.7), (3.8)}$$

The regression coefficients are calculated as:

$$a_{i0} = \frac{\sum Y_i}{N} \; ; a_{ip} = \frac{\sum X_p Y_i}{N} \; ; a_{ipq} = \frac{\sum (X_p X_q) Y_i}{N} \; ; a_{i123} = \frac{\sum (X_1 X_2 X_3) Y_i}{N} \text{ ------- (3.9 ~ 3.12)}$$

where, $p = 1,2,3$, $q = p+1,\cdots 3$, $p \neq q$, the coefficient a_{i0} represents the average value obtained from these experiments conducted at base-level as indicated in tests 9 ~ 11 of Table 3-7. Coefficients a_{i1}, a_{i2}, and a_{i3} give the effects of reduction time, temperature, and CO content of reducing gas, respectively. Coefficients a_{i12}, a_{i13}, and a_{i23} refer to the interactive effect of two of the parameters investigated in this work, and a_{i123} shows the interactive effect of all three parameters. The results for various tests of 2^3 full factorial experiments are summarized in Table 3-8.

Table 3-8 Test result of 2^3 factorial experiments

Test	X_1	X_2	X_3	% Fe removed		Mn/Fe		% Mn lost	
				Expe.[1]	Corr.[2]	Expe.[1]	Corr.[2]	Expe.[1]	Corr.[2]
1	1	1	1	48.7	48.5	16.0	15.6	5.2	4.6
2	1	-1	1	25.3	27.6	10.8	12.0	3.0	2.3
3	-1	-1	1	23.2	25.8	12.2	11.5	2.6	2.2
4	-1	-1	-1	14.6	18.2	11.8	11.0	1.8	1.5
5	-1	1	-1	31.0	32.6	14.6	12.9	3.8	3.2
6	1	1	-1	33.3	34.8	12.4	13.2	2.8	3.4
7	-1	1	1	31.8	33.6	12.9	13.0	4.2	3.0
8	1	-1	-1	24.2	26.9	13.7	11.7	2.8	2.3
9	0	0	0	30.9	31.0	12.6	12.6	2.8	2.8
10	0	0	0	31.0	31.0	12.5	12.6	2.8	2.8
11	0	0	0	31.0	31.0	12.7	12.6	2.8	2.8

1: Experimental data, 2: Correlated value calculated from regression equations.

Based on these test results, the regression equations, which represent the effects of experimental parameters and their interactions on the efficiency of prereduction and magnetic separation, are developed as follows:

$$Y_1= 31.0+3.44X_1+6.39X_2+2.89X_3+0.82X_1X_2+0.72X_1X_3+0.79X_2X_3+2.45X_1X_2X_3 \text{---(3.13)}$$

$$Y_2= 12.6+0.52X_1+1.05X_2+0.40X_3+0.22X_1X_2+0.25X_1X_3+0.21X_2X_3+0.31X_1X_2X_3 \text{---(3.14)}$$

$$Y_3= 2.8+0.34X_1+0.74X_2+0.21X_3+0.12X_1X_2+0.08X_1X_3+0.03X_2X_3+0.26\ X_1X_2X_3 \text{---(3.15)}$$

The three base-level tests give highly consistent results, implying a good reproducibility of the experiments.

From the regression Equations (3.13) ~ (3.15), we can learn that within the ranges of different experimental parameters selected, all of the experimental parameters have significant effect on the efficiency of prereduction and magnetic separation. With increasing temperature, reduction time, and CO content, the amount of removed iron and Mn/Fe ratio achieved by magnetic separation are improved. The amount of manganese lost during the magnetic separation also increases. Among these parameters studied in this work, temperature has the strongest effect in the range tested, followed by reduction time and CO content. In addition, these regression equations also indicate that all of the interaction effects are positive for the removal of iron, improvement of Mn/Fe ratio as well as manganese loss, but the significance of interaction effect is much smaller than the effect of each single experimental parameter. The correlated values, reproduced from the regression equations, are listed in Table 3-8, and they are in a good agreement with the experimental data.

CHAPTER 4

KINETICS STUDY ON THE PREREDUCTION OF MANGANESE ORE BY CO

4.1 Experimental

4.1.1 Sample preparation

It is obvious that the kinetics of prereduction is closely related to the reduction extent achieved in the experiment, which is defined as percentage removal of the removable oxygen, i.e., the oxygen present in the ore associated with manganese and iron. Prior to reduction, the "LP" sample particles were calcinated at 900˚C in argon so as to make the weight loss totally attributable to the reduction of the oxides.

The synthetic samples, used to study the effect of impurities on reduction process, were prepared by mixing relatively pure oxides. All of these oxides are A.R. quality chemical reagents except Mn_3O_4, which was prepared by thermal decomposition of 99.5% pure MnO_2 chemical reagent particles in argon atmosphere at 950˚C. The weight loss curve during the heating and the XRD pattern of prepared Mn_3O_4 particles are shown in Figure 4-1 and Figure 4-2, respectively.

Based on Figure 4-1, the weight loss fraction achieved by the heating was calculated to be 12.31%, this is in a good agreement with the theoretical value (12.27%) corresponding to the decomposition of MnO_2 to Mn_3O_4. Moreover, XRD test results shown in Figure 4-2 also indicates the prepared Mn_3O_4 sample is suitable for this study.

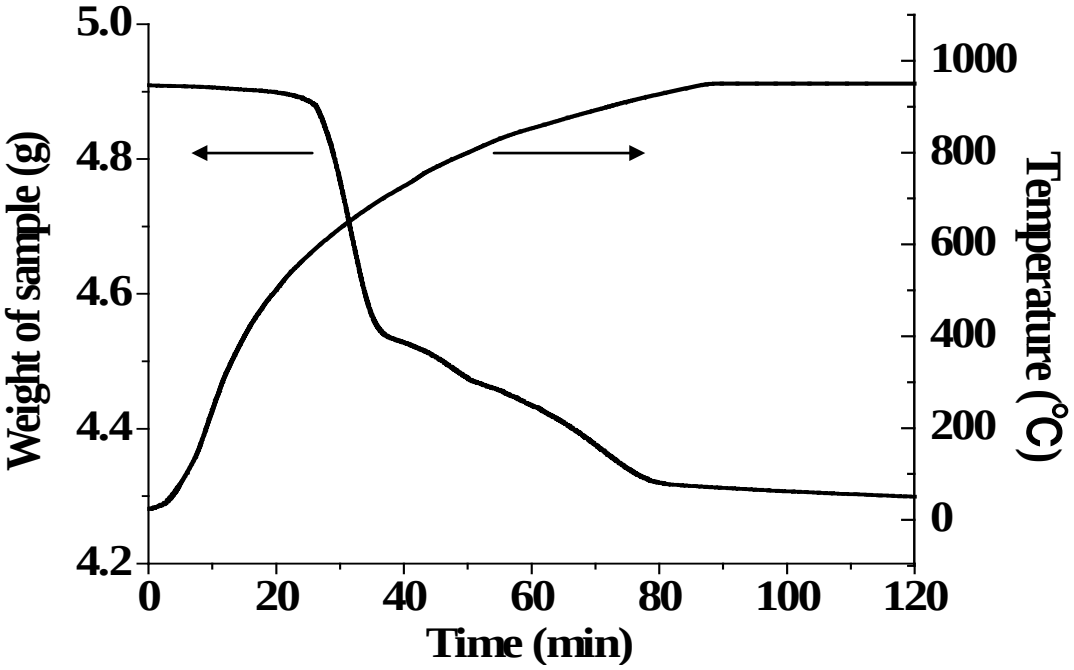

Figure 4-1 Time-weight loss curve and temperature profile for the thermal decomposition of MnO_2 reagent particles

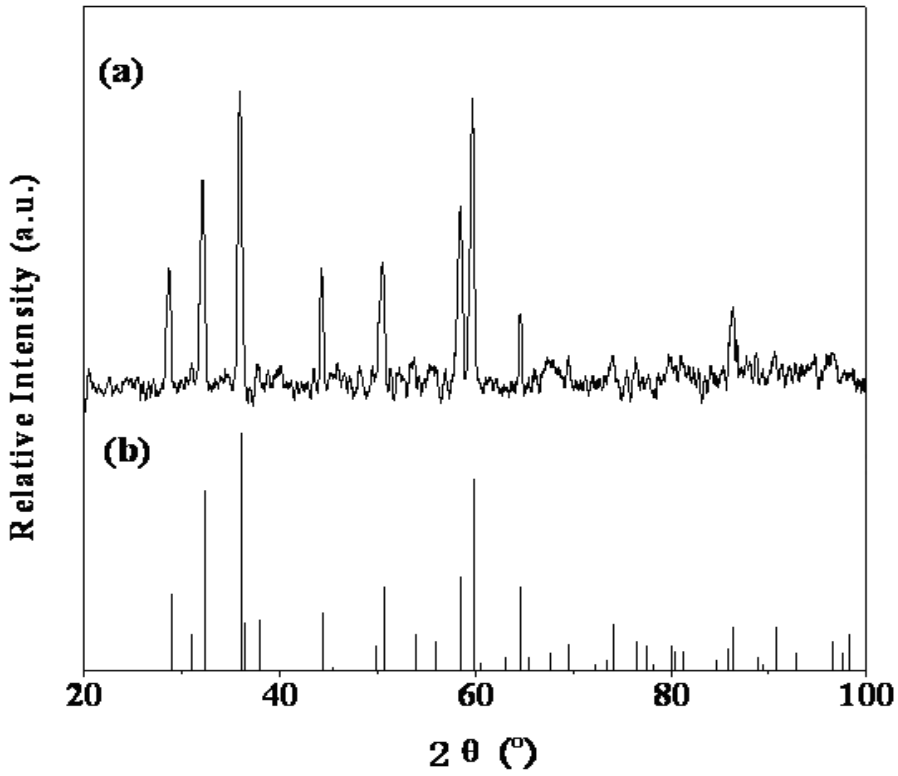

Figure 4-2 XRD test results: (a) XRD pattern of as-prepared Mn_3O_4 particles, (b) the corresponding standard XRD pattern for Mn_3O_4 (PDF#24-0734)

4.1.2 Procedure and apparatus

The reduction of calcinated sample was conducted by a continuously recording electro-balance (Cahn, RTL #7000 for 110v 60Hz, Cahn Instruments, California, USA), which is schematically shown in Figure 4-3, using mixtures of CO and CO_2 with different CO/CO_2 ratios. The reactor used for reduction was a vertical quartz tube (internal diameter: 45 mm, outside diameters: 48 mm, length: 850 mm), and the total gas flow rate was maintained at 1.5 NL/min. In order to ensure good access of the reducing gas to the sample particles, a shallow crucible was used as sample holder. As a result, the resistance from the diffusion of reducing gas through the section above the sample layer as well as between the particles could be neglected. A temperature of 600˚C was used for most of the experimental work, although temperatures in the range of 400 ~ 700˚C were included to determine the effect of temperature. The particle size tested in this work was less than 1000 μm.

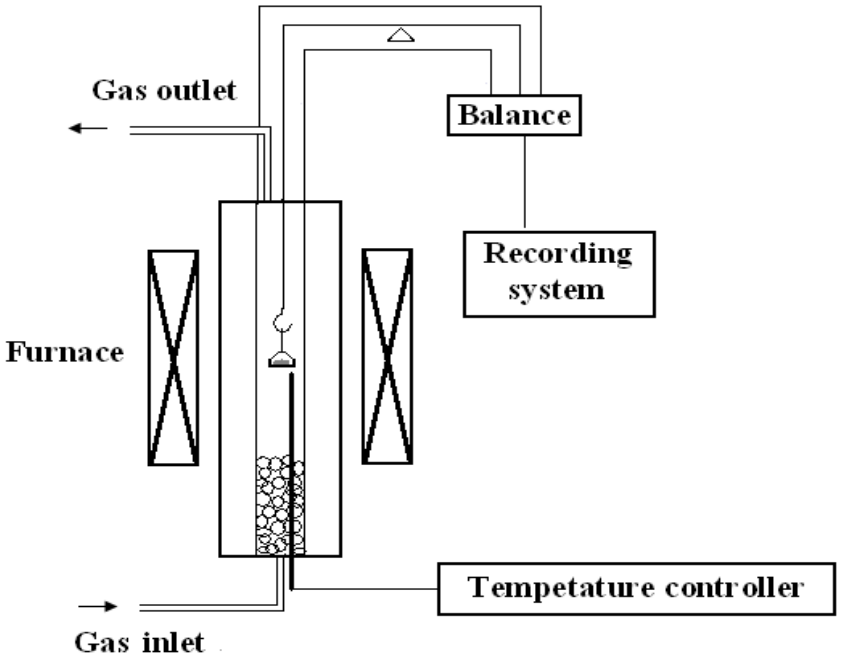

Figure 4-3 Schematic diagram of Cahn-balance apparatus

During the reduction, the weight of sample was continuously recorded by the Cahn-balance system, and the data were converted to reduction extent by Equation 4.1:

$$X = \frac{W_i - W_t}{W_i - W_f} \times 100\,\% \text{ ---------- (4.1)}$$

where, X is reduction extent, W_i and W_f refer to the initial weight of calcinated sample and the weight of final reduced particles, respectively, W_t is the specific sample weight at certain reduction time.

4.1.3 Reproducibility of experiments

The reproducibility of experimental system employed in this work was tested by the reduction of calcinated sample under an identical experimental condition (temperature: 550˚C, particle size: 105 ~ 150 μm, CO/CO_2: 30/70), and the test results for weight loss and reduction extent as a function of time are given in Figure 4-4 and Figure 4-5, respectively.

Figures 4-4 and 4-5 indicate that there is no big difference between the original result and the repeat one, neither in the weight loss nor in the reduction extent, implying a good reproducibility, which is mainly contributed by the good uniformity in chemical and physical properties of sample particles used in this work, and the strict control on experimental conditions.

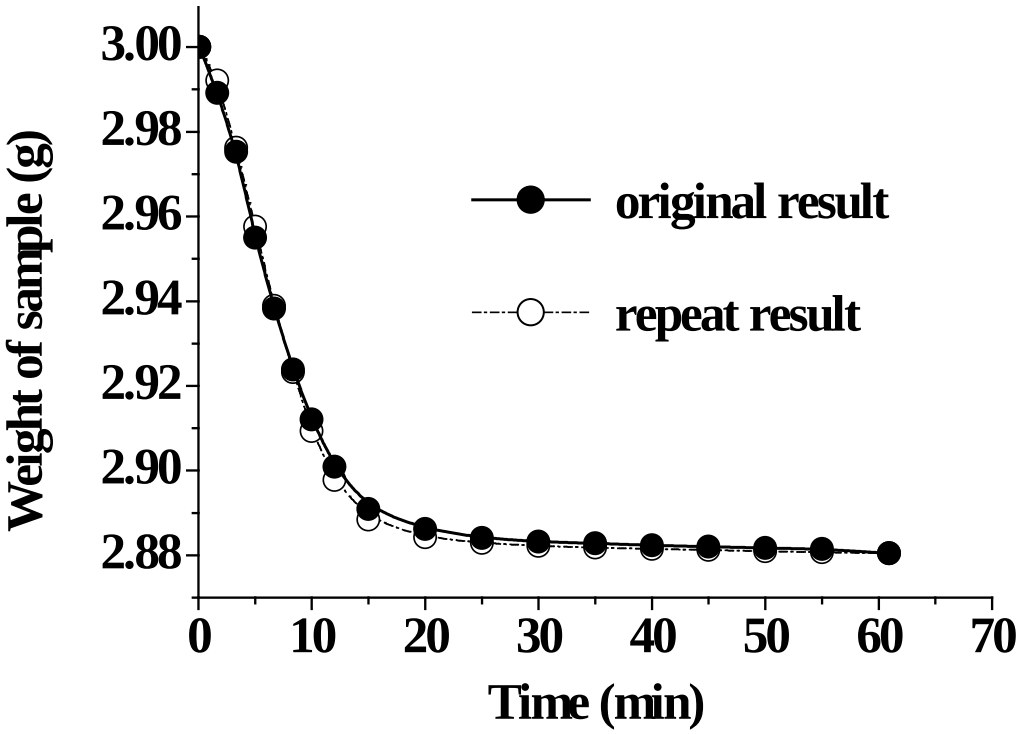

Figure 4-4 Reproducibility test result of weight loss

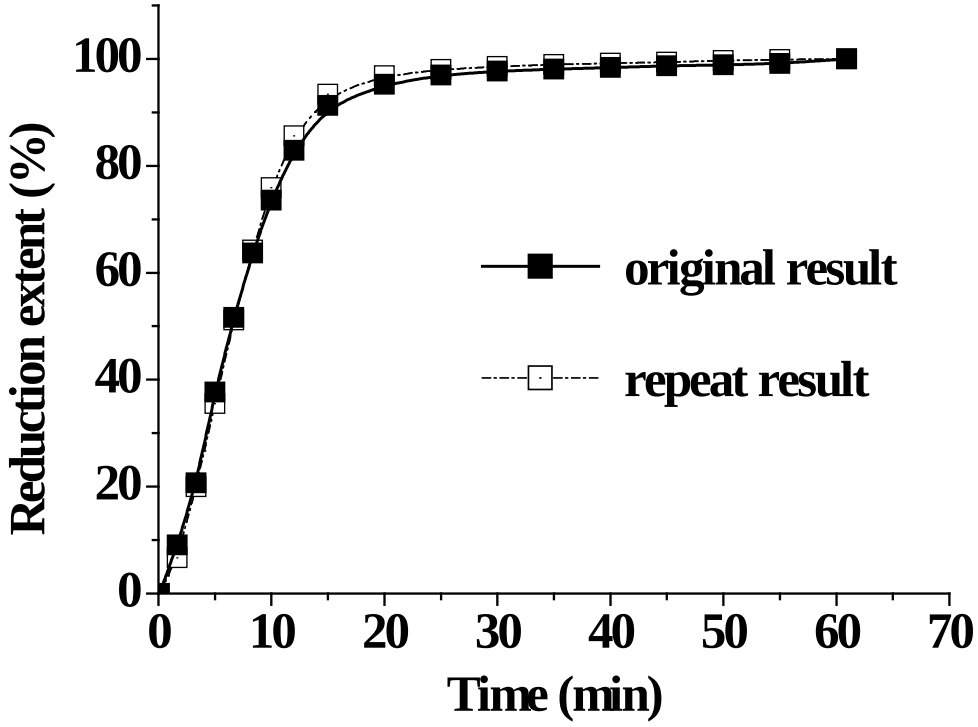

Figure 4-5 Reproducibility test result of reduction extent

4.2 Results and discussion

4.2.1 The reduction progress of “LP” ore

In order to study the reduction progress of calcinated “LP” manganese ore, partially reduced samples taken in the progress of reduction at 500˚C with the mixture gas of CO and CO_2 (CO/CO_2=30/70) were subjected to XRD analysis. The weight loss extents, corresponding to different reduction times, are marked in Figure 4-6, and the XRD patterns of samples with different reduction times are shown in Figure 4-7.

The XRD test results indicate that, after calcination, the manganese oxides contained in the original “LP” manganese ore are decomposed to Mn_3O_4, while iron oxide remains as Fe_2O_3. When a calcinated sample was exposed to the reducing gas for 5 minutes, Mn_3O_4 was partly reduced to MnO, but the phase of Fe_3O_4 was not observed. This fact might suggest that the reduction of Mn_3O_4 precedes the reduction of Fe_2O_3 in this case. After 15 minutes, the strengths of peaks corresponding to the phase of Mn_3O_4 decreased significantly, and the Fe_3O_4 phase was also detected. When the sample was reduced for 40 minutes, most of the manganese oxides and iron oxides were converted to MnO and Fe_3O_4, respectively. The final sample, reduced for 60 minutes, was composed of MnO, Fe_3O_4, SiO_2, and Al_2O_3. The XRD patterns presented in Figure 4-7 also show that, during the reduction, there is no chemical phase change for the SiO_2 and Al_2O_3, and thus the weight loss achieved in the reduction of calcinated “LP” manganese ore is due entirely to the reduction of manganese oxide and iron oxide as expected.

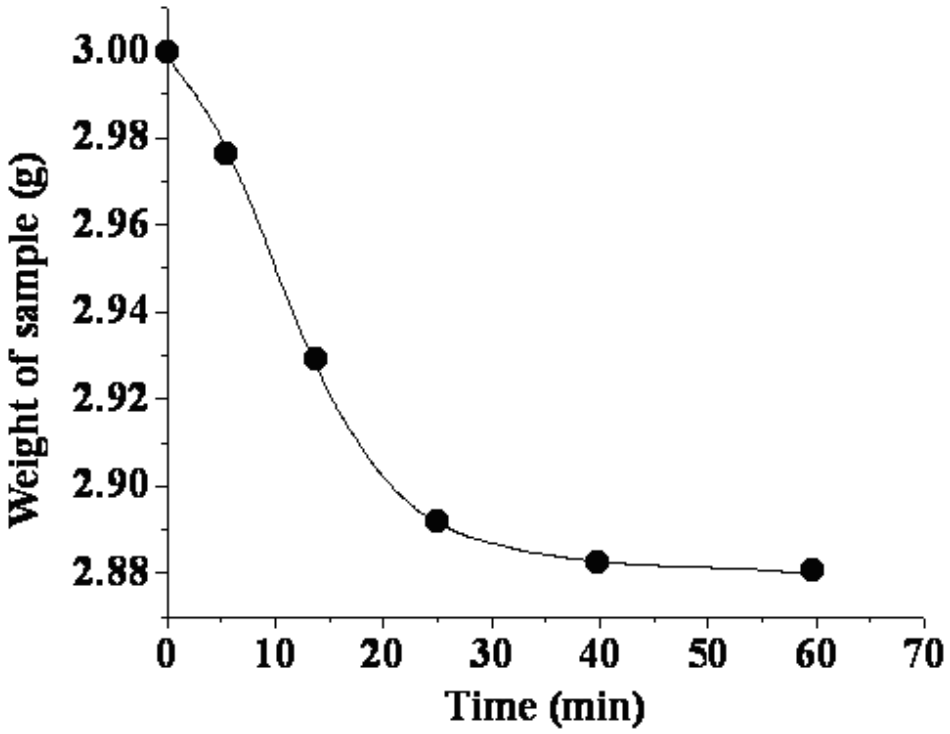

Figure 4-6 Time-weight loss curve for the reduction of calcinated “LP” ore at 500˚C, CO content = 30 vol%

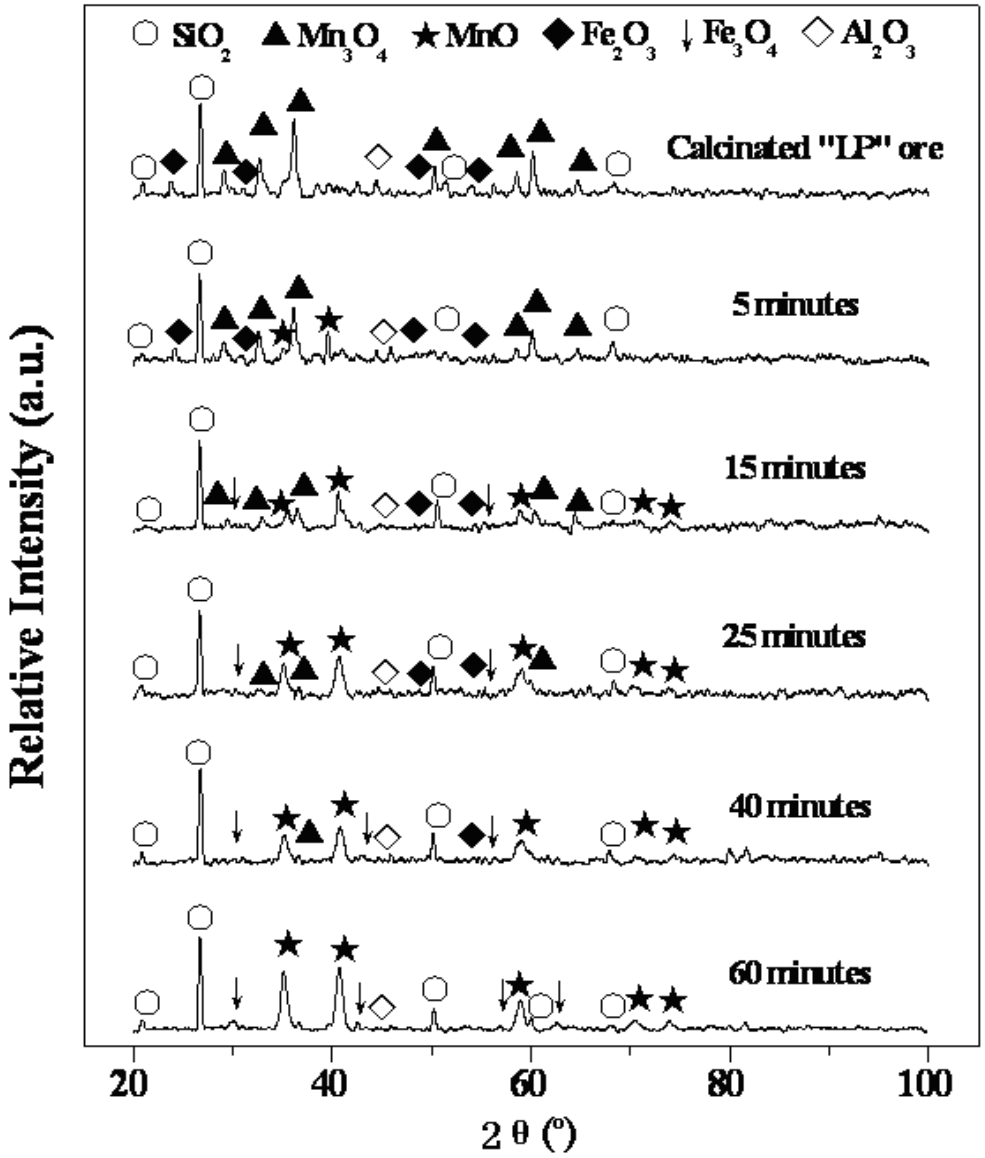

Figure 4-7 XRD patterns of reduced “LP” samples with different reduction times

4.2.2 The effect of particle size

In order to investigate the effect of particle size on the reduction of calcinated “LP” ore, several experiments were conducted at 600˚C, using a mixture gas of CO and CO_2 (CO/CO_2=30/70). The curves of weight loss and reduction extent versus time for various calcinated samples with different particle size ranges are presented in Figure 4-8 and Figure 4-9, respectively.

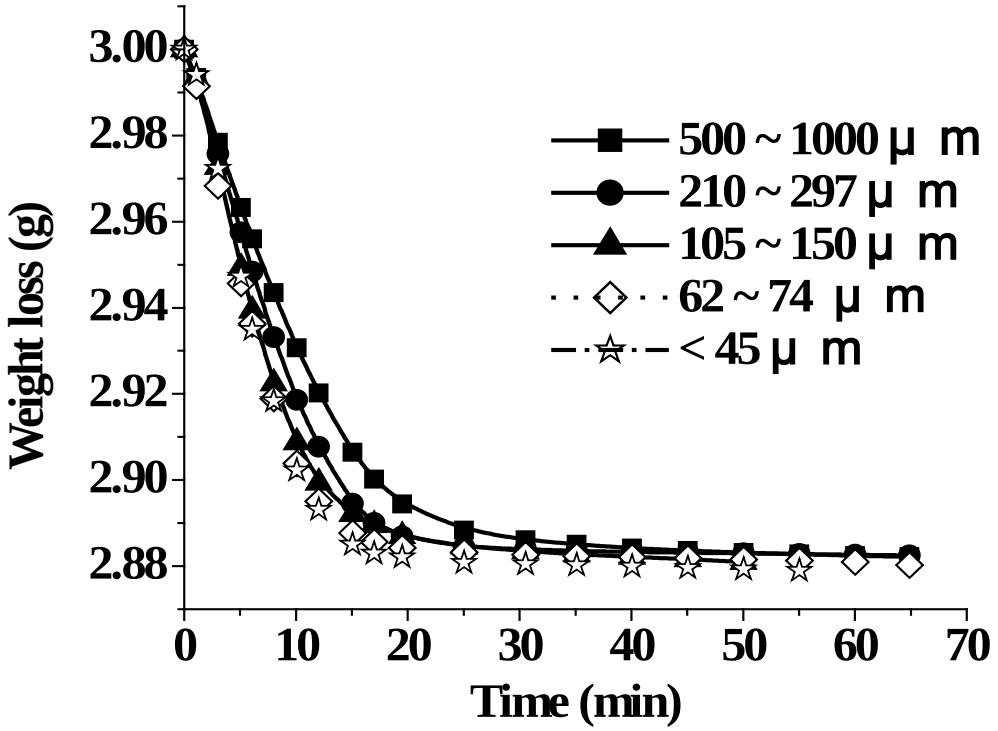

Figure 4-8 Time-weight loss curves for the reduction of calcinated "LP" ore at different particle size ranges, T= 600˚C, CO content = 30 vol%

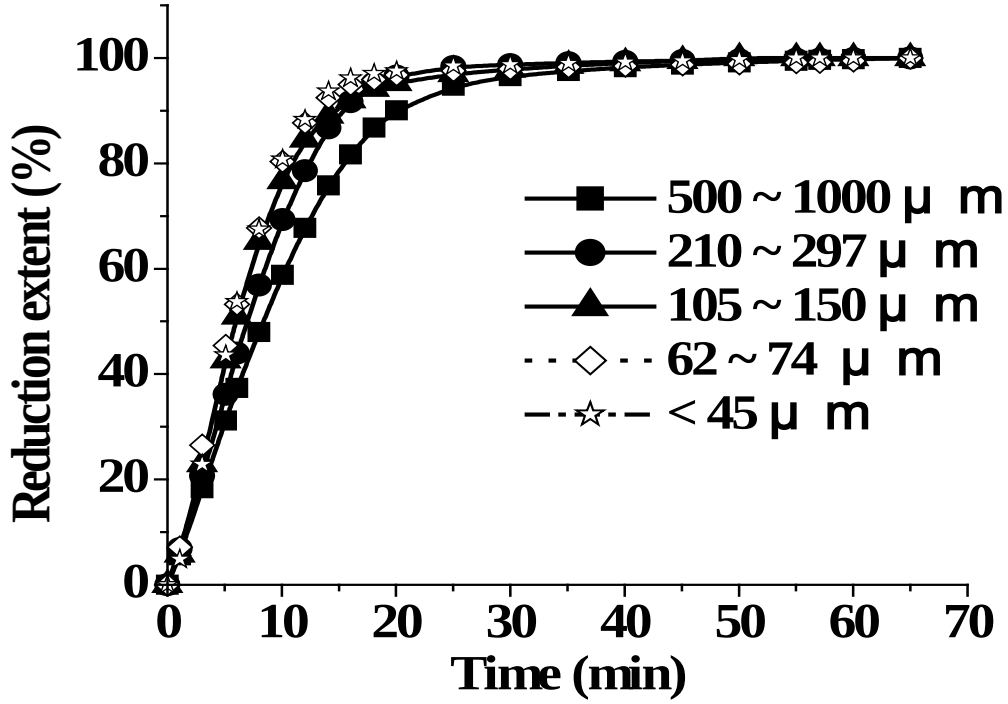

Figure 4-9 Time-reduction extent curves for the reduction of calcinated "LP" ore at different particle size ranges, T= 600˚C, CO content = 30 vol%

As shown in the above figures, all of the time versus reduction curves for various particle size ranges at 600˚C consist two parts. The initial stage, during which the rate of reduction is very fast, is followed by a longer stage, which is characterized by a marked decrease in the slope of the curve, and thus in the rate of reduction. This is probably due to the change in rate-controlling step. These curves also indicate that the reduction rate increases with decreasing particle size. When the particle size decreases to around 150 μm, the effect of particle size becomes smaller, and the initial stage of reduction even tends to be particle size independent when the particle size of sample further decreases to 74 μm. This may be caused by the microstructural change occurring in the process of reduction, and thus, both the calcinated and partially reduced particles, within the size range between 500 and 70 μm are tested by SEM, and the test results are given in Figures 4-10 and 4-11.

Although the calcinated “LP” particles are dense as shown in Figures 4-10 (1) ~ (4), it could be clearly observed from the SEM pictures of partially reduced samples, as shown in Figures 4-11 (1) ~ (4), that cracks formed during the reduction, which is probably due to thermal stress. As reaction may take place significantly at these cracks where the reducing gas has access, these cracks would result in a decrease in effective or practical particle size of sample, and thus this may account for the result that the effect of particle size on the reduction rate is not as notable as expected.

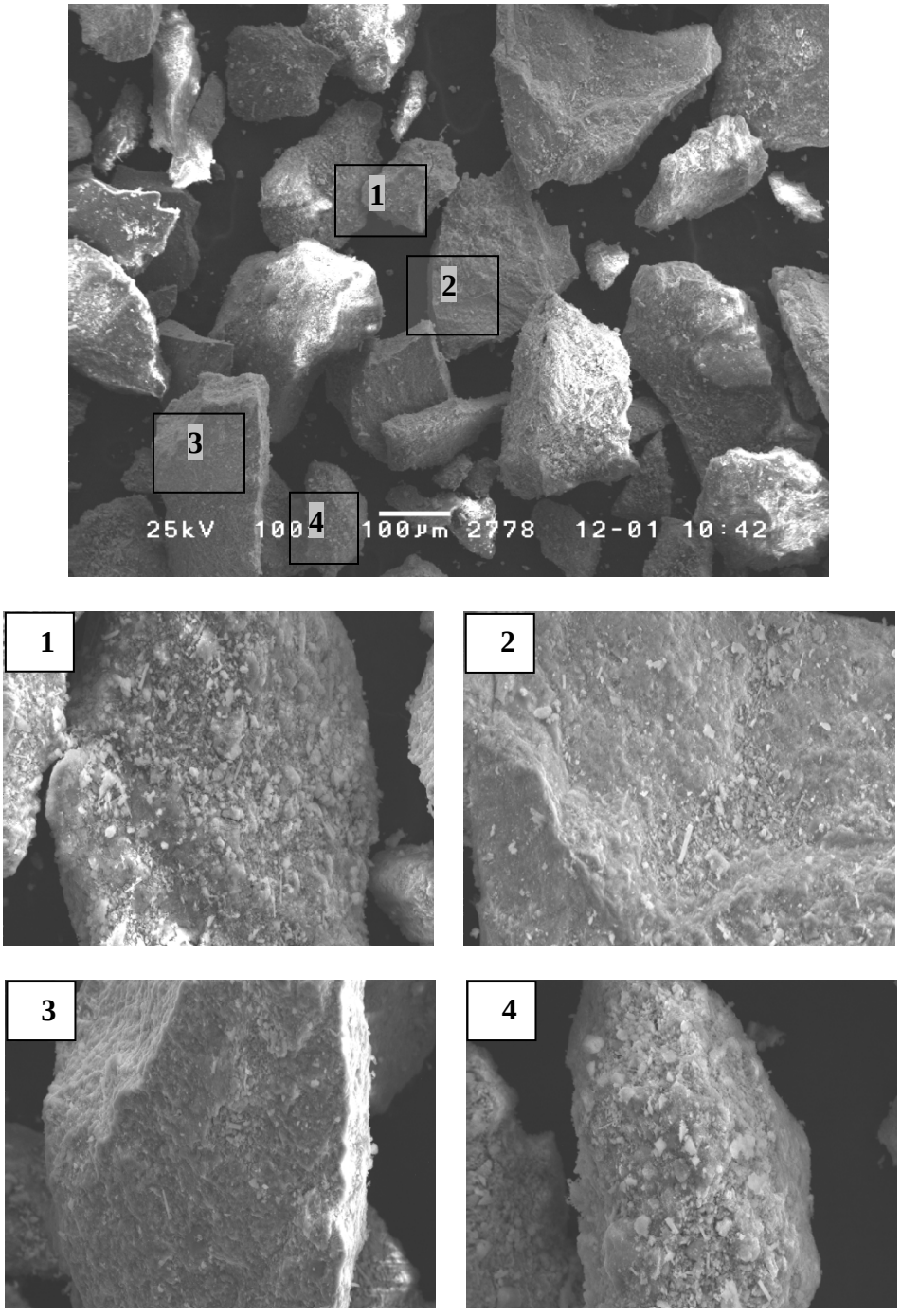

Figure 4-10 SEM pictures for “LP” sample particles, calcinated at 900˚C

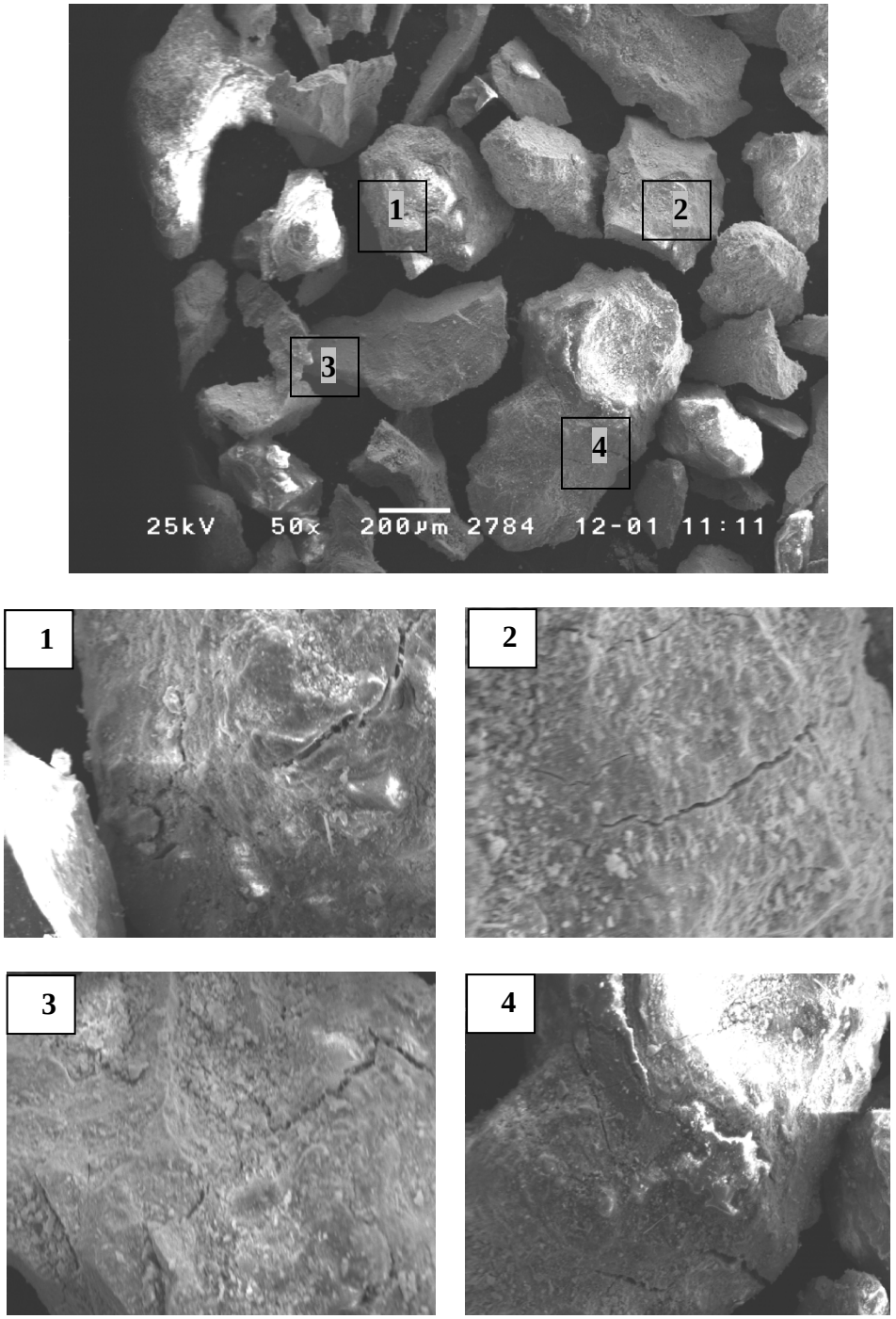

Figure 4-11 SEM pictures for partially reduced “LP” sample particles
T= 600˚C, CO content = 30 vol%

4.2.3 The effect of temperature

The effect of temperature was studied in the range from 400 to 700˚C, both nonisothermal and isothermal tests were conducted in this work, and the specific values of temperature tested in isothermal reduction experiments are marked in Figure 4-12. The reducing gas was a mixture gas of CO and CO_2 at the volume ratio of CO/CO_2 = 30/70. In order to minimize the interference effect of particle size, only the sample particles in the range of 105 ~ 150 μm were used.

The curves for weight loss and reduction extent versus time obtained by various isothermal tests are demonstrated in Figure 4-13 and Figure 4-14, respectively.

The effect of increased temperature is an increase in the rate of reduction. At 400˚C the reduction rate is very slow. This is in good agreement with the test result of non-isothermal reduction, which indicates the significant reduction does not start until the temperature reaches around 440˚C, as shown in Figure 4-15.

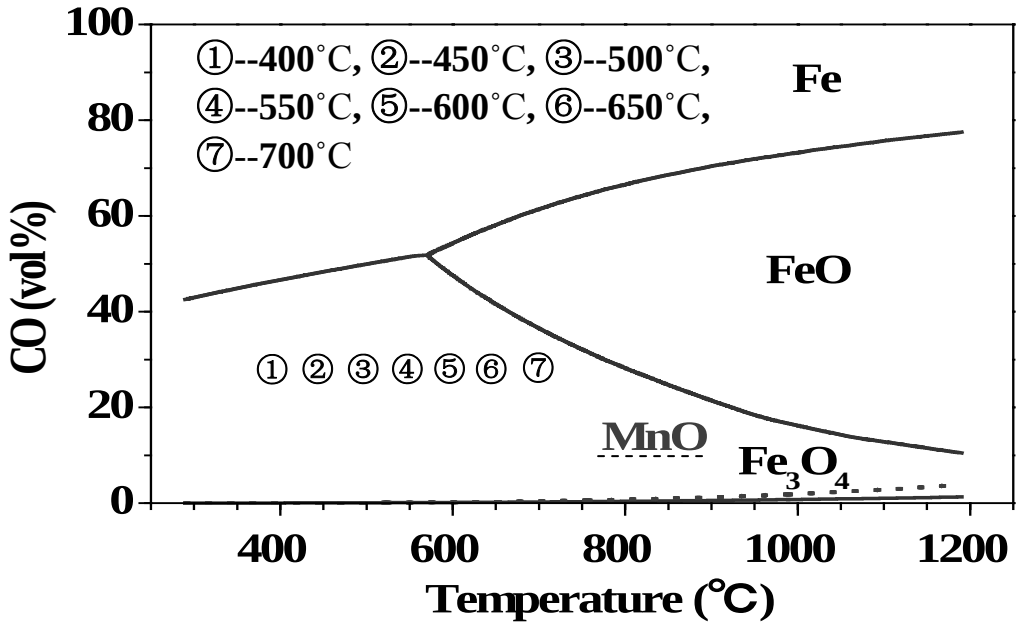

Figure 4-12 Experimental conditions for temperature effect on reduction of calcinated "LP" ore

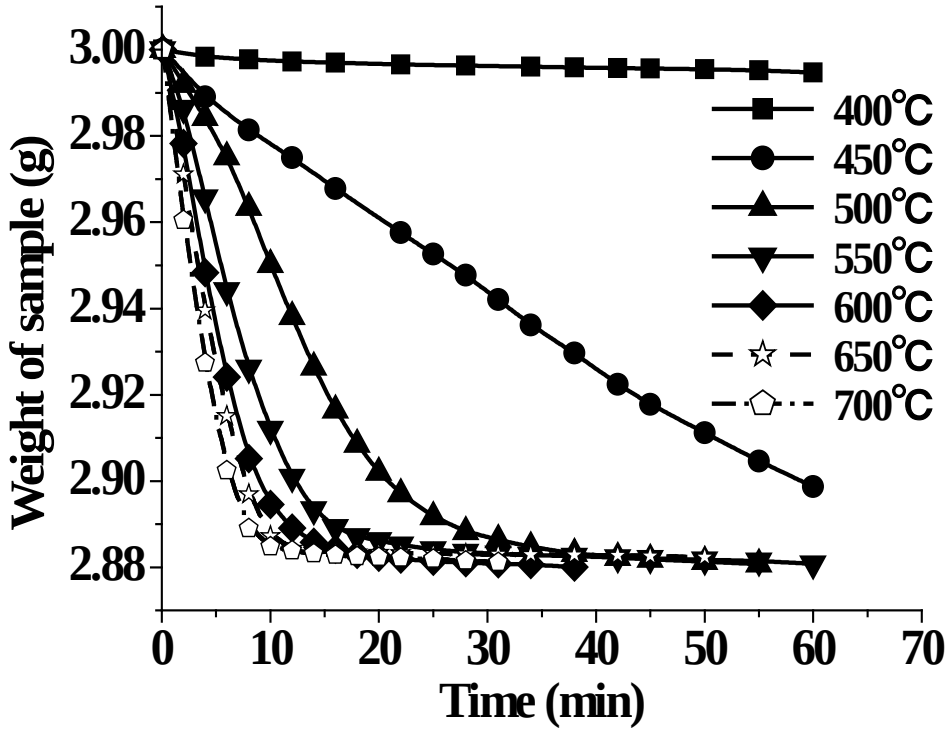

Figure 4-13 Time-weight loss curves for the isothermal reduction of calcinated “LP” ore at different temperatures, CO content = 30 vol%

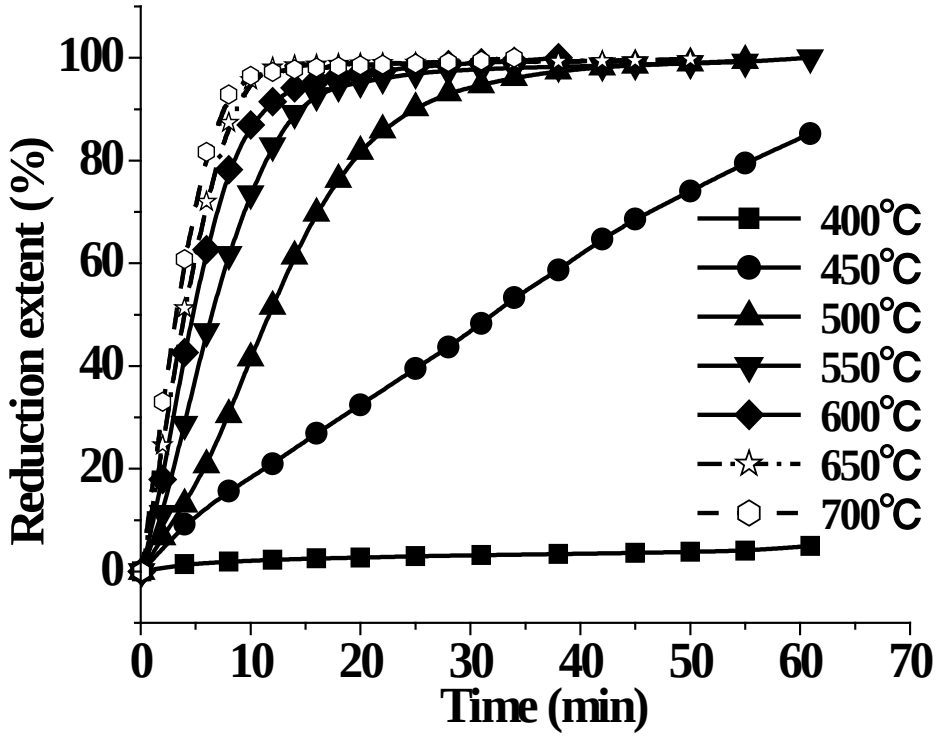

Figure 4-14 Time-reduction extent curves for the isothermal reduction of calcinated “LP” ore at different temperatures, CO content = 30 vol%

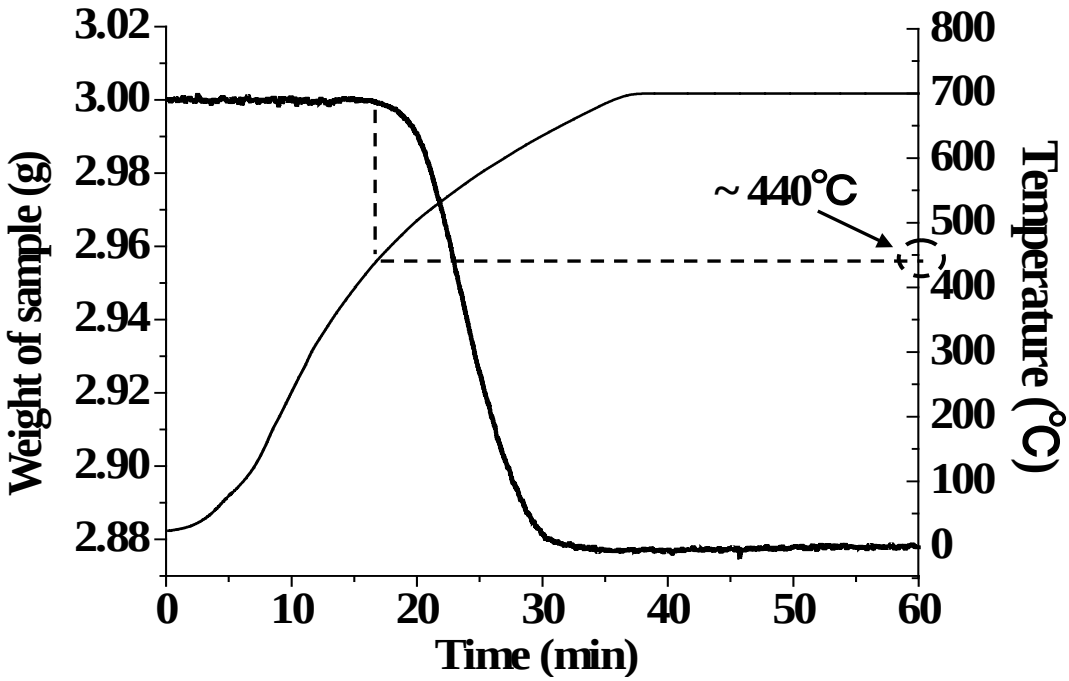

Figure 4-15 Time-weight loss curves for the nonisothermal reduction of calcinated "LP" ore, CO content = 30 vol%

Figures 4-13 and 4-14 also show that, in the temperature range of 450 ~ 600˚C, the rate of reduction increases distinctly as the temperature increases, and all of the corresponding curves tend to level out after a certain time.

4.2.4 The effect of CO content

To study the effect of CO content on the reduction, experiments were conducted at four different CO/CO_2 volume ratios between 10/90 to 40/60, as indicated in Figure 4-16. Reduction temperature was controlled at 600˚C, and the size was 105 ~ 150 μm.

According to the test results of reduction at different CO contents, as shown in Figures 4-17 and 4-18, all the reduction curves obtained at different CO/CO_2 ratios tend to level off after a certain time. Moreover, a higher CO content results in a higher reduction rate. This effect is especially notable when the CO content changes from 10 to 30 vol%.

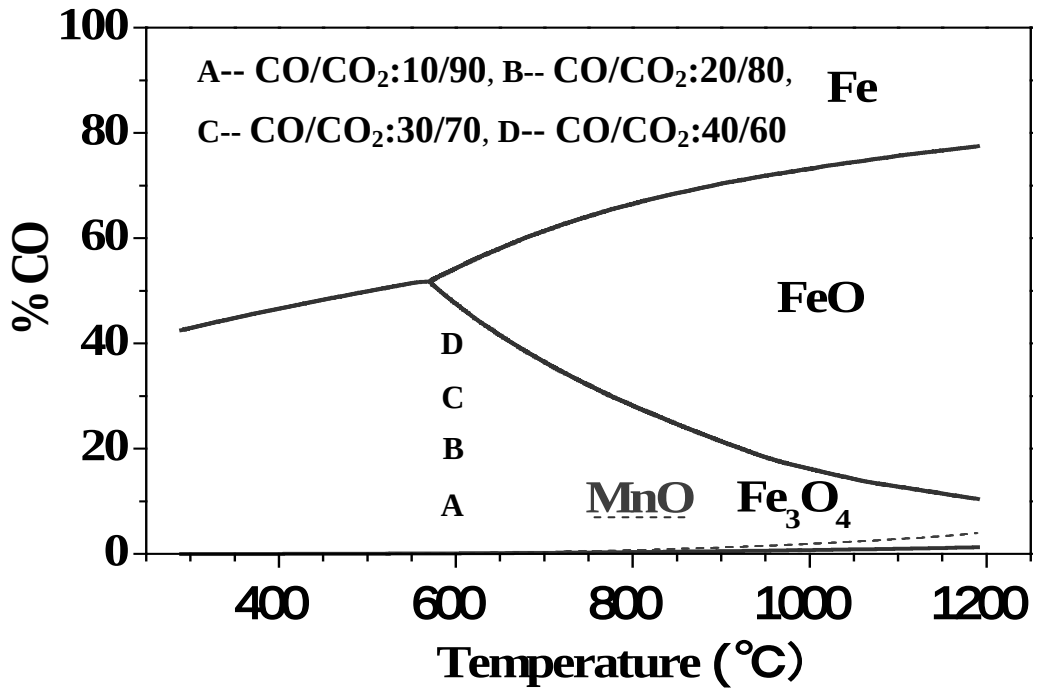

Figure 4-16 Experimental conditions for CO content effect on reduction of calcinated "LP" ore

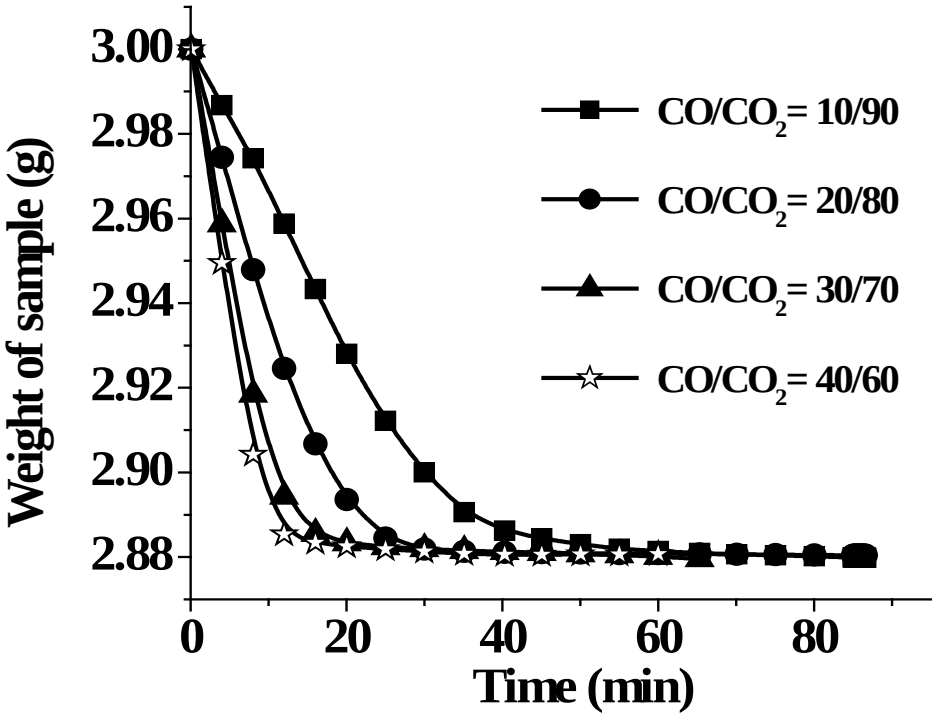

Figure 4-17 Time-weight loss curves for the reduction of calcinated "LP" ore at different CO contents, T = 600˚C

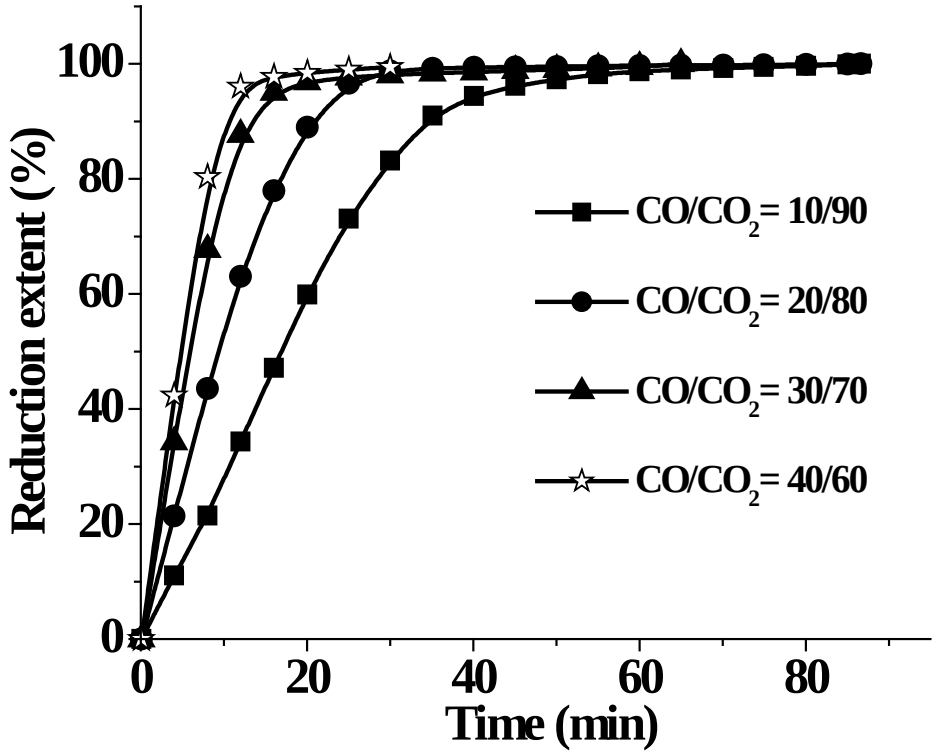

Figure 4-18 Time-reduction extent curves for the reduction of calcinated "LP" ore at different CO contents, T = 600˚C

4.2.5 The effect of bed depth

The effect of bed depth was studied at 600˚C with a mixture gas of CO and CO_2 at the volume ratio of CO/CO_2 = 30/70, the particle size of sample used in these tests was in the range of 105 ~ 150 μm. For these experiments, the bed depth, varying from 0.1 cm to 0.4 cm, was controlled by changing the amount of sample particles contained in the crucible. The reduction curves obtained for different bed depths are shown in Figure 4-19.

The experiment result shows that, although slight derivation occurs in the terminal part of reduction curves for different bed depths, up to 90% of reduction extent, the reduction rate is almost independent of bed depth.

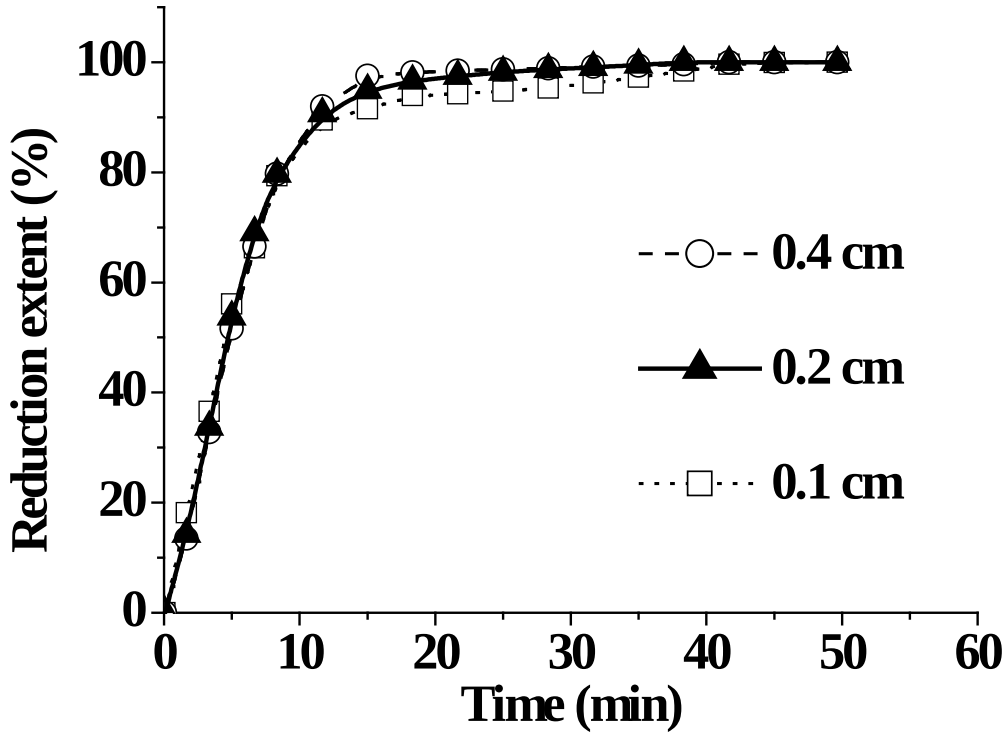

Fig 4-19 The effect of bed depth on the reduction of calcinated “LP” ore,
T = 600˚C, CO content = 30 vol%

As stated in section 4.1.2, the crucible used in the study is very shallow, and the reducing gas is allowed good access to the sample layer. Based on this fact, the result obtained in these tests may indicate that the interior spacing between different sample particles loaded in the crucible is so large that the reducing gas can access the sample particles at different depths very readily, the reactive atmosphere throughout the entire bed is approaching uniform, and thus it could be concluded that the bed depth, in this case, has no significant effect on the reduction of sample ore with the experimental apparatus employed in this work. This lends support to the reliability of the following kinetics analysis.

4.2.6 Kinetics analysis

The rate of overall reduction can be controlled by diffusion, chemical reaction and nucleation and growth. Assume the sample particles involved in this work are approximately equidimensional particles with uniform reactivity in different orientations, and then, if the reaction is controlled by pore diffusion, the reaction time would be proportional to $[1 + 2(1-X) - 3(1-X)^{2/3}]$, where "$X$" is the reduction extent; if the overall reaction is controlled by the chemical reaction, the reaction time would be proportional to $[(1 - (1-X)^{1/3})]$; in addition, according to Avrami equation, if it is controlled by nucleation and growth, plots of $\{ln [-ln (1-X)]\}$ versus $ln\ t$ at different temperatures should be straight lines. [24~26] Since there are many uncertainties for the terminative part of reduction, only the data below the reduction extent of 0.95 ($X \leq 0.95$) were used for plotting and analysis. The plots of $[(1 - (1-X)^{1/3})]$ versus time, $[1 + 2(1-X) - 3(1-X)^{2/3}]$ versus time, and $\{ln [-ln (1-X)]\}$ versus $ln\ t$ are present in Figures 4-20 ~ 4-22, respectively.

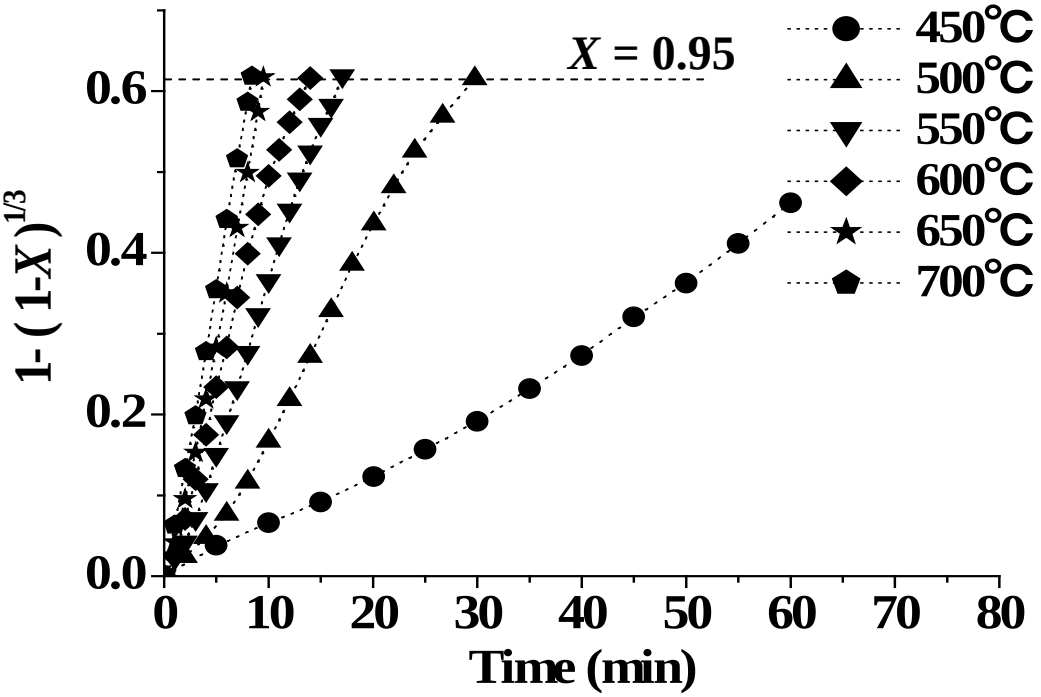

Figure 4-20 Plots of $[1 -(1-X)^{1/3}]$ versus time at various temperatures, CO content = 30 vol%

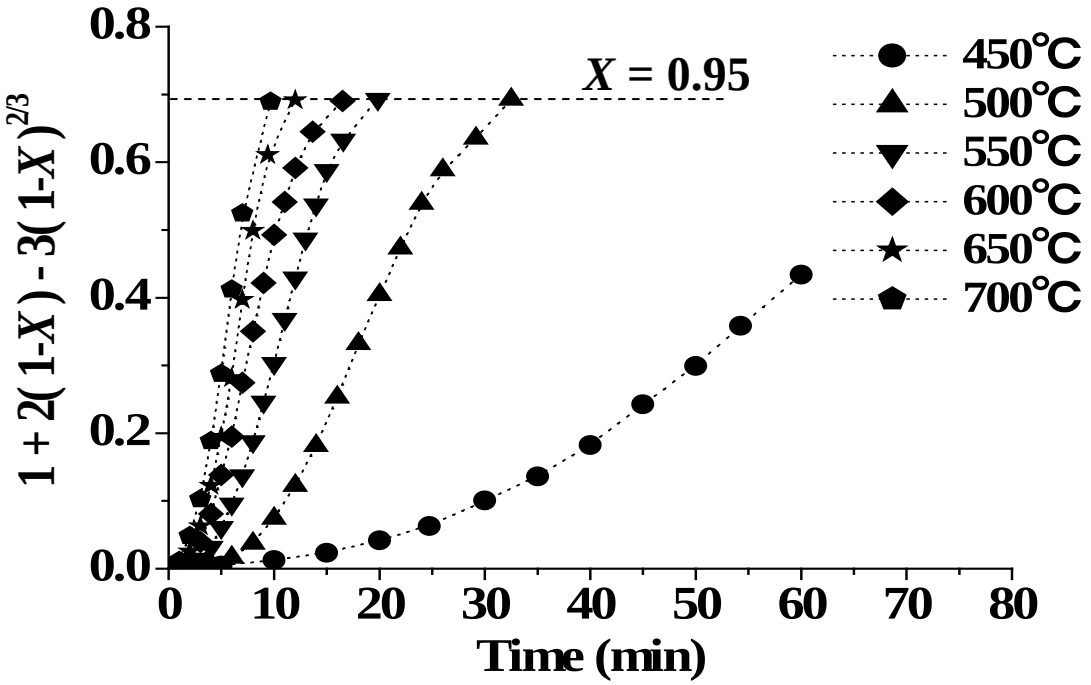

Figure 4-21 Plots of $[1 + 2(1-X) - 3(1-X)^{2/3}]$ versus time at various temperatures, CO content = 30 vol%

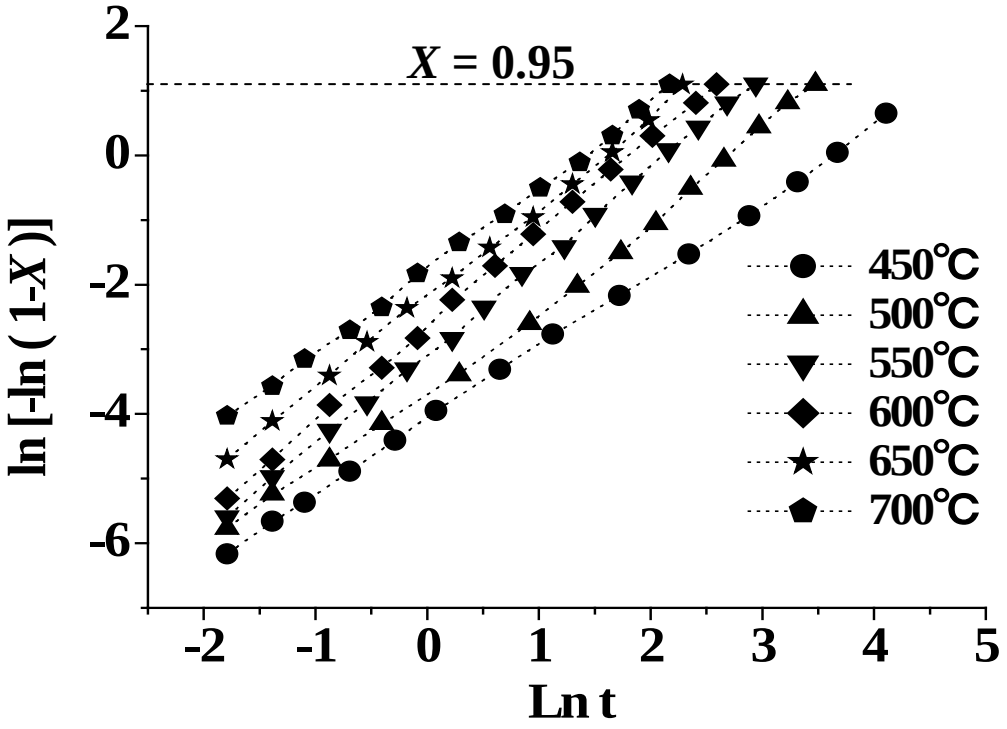

Figure 4-22 Plots of *{ln [−ln (1−X)]}* versus *ln t* at various temperatures, CO content = 30 vol%

As demonstrated in the above three figures, this reduction process is more likely to be chemical reaction controlled or nucleation and growth controlled. In this case, considering the size of sample particle used in the isothermal reduction experiments is as small as 105 ~ 150 μm, during the reduction, the particle size is probably not large enough for the formation of distinct continuous interface between reactant layer and product layer, which is generally required for the topochemical reduction mechanism. Besides, as shown in Figure 4-11, cracks are formed in the sample particle during the reduction. For the particle containing cracks, the reaction taking place within these cracks may also result in the formation of several cores during the reduction progress for a single sample particle, and this is another reason why the topochemical reduction

mechanism is not the most suitable for this reduction process. Therefore, this reduction process is better described by nucleation and growth, expressed by:

$$[-ln(1-X)]^{1/n} = k_{app}\, t \quad (4.2)$$

where, X is reduction extent, n is a constant, k_{app} refers to apparent rate constant, and k_{app} contains the effect of particle pressures according to

$$k_{app} = k\,[p_{co}^{\,m} - (p_{co2} / K)^{\,m}] \quad (4.3)$$

in which k is effective rate constant, K is equilibrium constant, m is reaction order, p_{co} and p_{co2} refer to partial pressure of CO and that of CO_2, respectively, and could be calculated by:

$$p = 0.85 \text{ atm} \times \text{vol\%}/100 \quad (4.4)$$

where 0.85 atm (1 atm = 101.3 kPa) is the local atmospheric pressure at Salt Lake City.

Since the value of equilibrium constant K (in this case, $K \geq 1.77 \times 10^{21}$) is so large that the term (p_{co2} / K) could be neglected, compared with the term of $p_{co}^{\,m}$, and the Equation 4.3 is further simplified as:

$$k_{app} = k\, p_{co}^{\,m} \quad (4.5)$$

Based on plots of $\{ln\,[-ln\,(1-X)]\}$ versus $ln\,t$ at various temperatures, which are shown in Figure 4-22, we can get the slope of each line, and the average value of the slope was further calculated, all of which are summarized in Table 4-1.

Table 4-1 Values of order parameter (n) at various temperatures, p_{co} = 0.255 atm

Temperature (˚C)	450	500	550	600	650	700	Average
Slope / n	1.05	1.34	1.29	1.42	1.29	1.18	1.26

It is clear from Table 4-1 that the value of slope, i.e., order parameter "*n*", is in the range of 1.05 ~ 1.42, which is an indication of one-dimensional nucleation. By setting the slope of each plot as the average value, "1.26", Figure 4-23 shows the modified regression line for various temperatures. The value of "$ln\ k_{app,T}$", where $k_{app,T}$ refers to apparent rate constant at different temperatures, can be calculated from the intercepts on Y-axis, and the calculated values of "$ln\ k_{app,T}$" are given in Table 4-2.

In a similar way, by linear regression of plots of $\{ln\ [-ln\ (1-X)]\}$ versus $ln\ t$ at various CO contents, the values of $ln\ k_{app,co}$, where $k_{app,co}$ refers to apparent rate constant at different CO contents, can be calculated from the intercepts on Y-axis of Figure 4-24, and obtained values of $ln\ k_{app,co}$ are summarized in Table 4-3.

Table 4-2 Values of $ln\ k_{app,T}$ at various temperatures, p_{co} = 0.255 atm

Temperature (˚C)	450	500	550	600	650	700
$ln\ k_{app,T}$	-4.66	-3.46	-2.76	-2.38	-1.99	-1.75

*$k_{app,T}$ in min^{-1}

Table 4-3 Values of $ln\ k_{app,co}$* at various CO contents, T=600˚C

CO/CO_2	10/90	20/80	30/70	40/60
p_{co} (atm)	0.085	0.17	0.255	0.34
$ln\ k_{app,co}$	-3.39	-2.76	-2.38	-1.95

*$k_{app,co}$ in min^{-1}

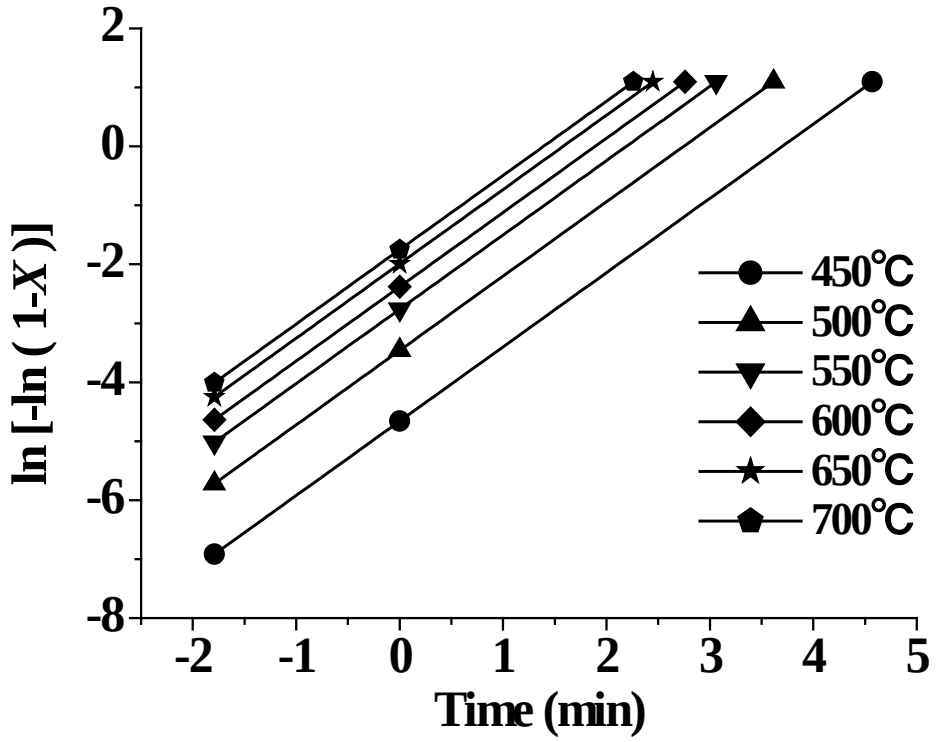

Figure 4-23 Modified plots of *{ln [−ln (1−X)]}* versus *ln t* at various temperatures

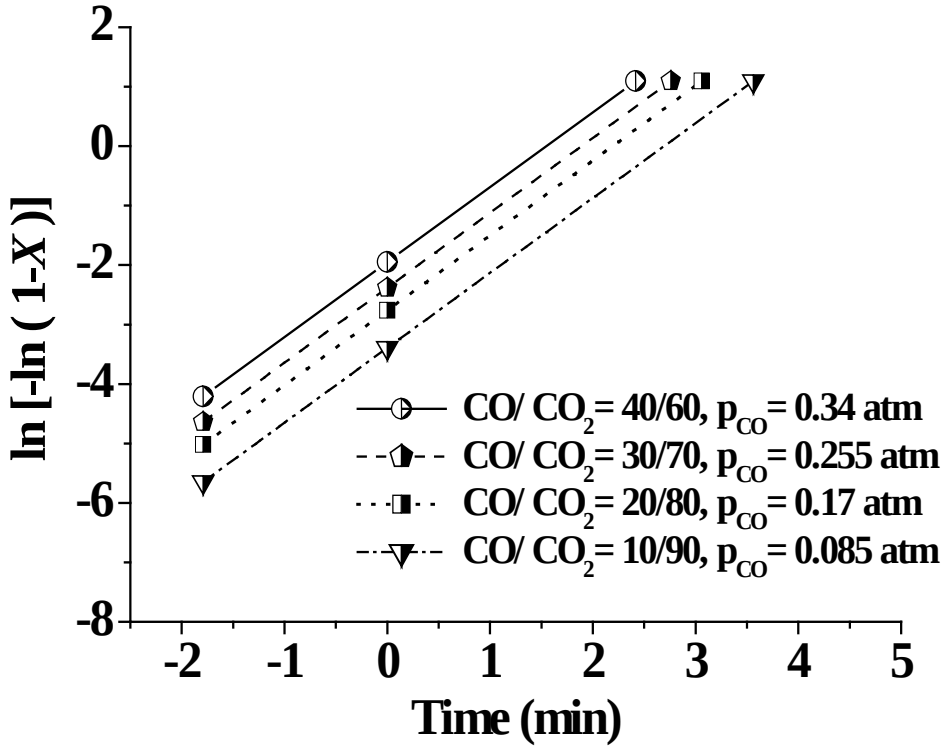

Figure 4-24 Plots of *{ln [−ln (1−X)]}* versus *ln t* at various CO contents, T = 600˚C

According to Equation 4.4, the value of "*m*" could be determined by the slope of the plot of $ln\ k_{app,co}$ as a function of $ln\ p_{co}$, as shown in Figure 4-25, and it comes to be 1.0, indicating a first order reaction with respect to CO partial pressure.

The values of $ln\ k_T$ for various temperatures can be further calculated by Equation 4.4, and calculated values of $ln\ k_T$ are given in Table 4-4.

Figure 4-26 shows the Arrhenius plot, the activation energy of nucleation estimated from the slope of this curve is around 66 kJ/mol.

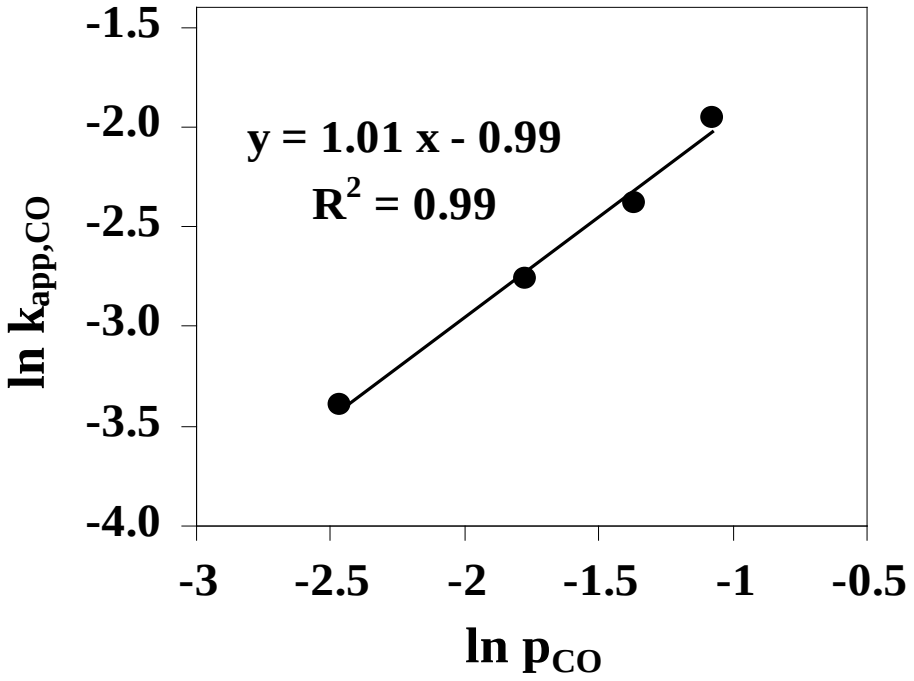

Figure 4-25 Plots of $ln\ k_{app,co}$ versus $ln\ P_{co}$ at various CO contents, T = 600˚C, ($k_{app,co}$ in min^{-1})

Table 4-4 Values of $ln\ k_T$ * at various temperatures, p_{co} = 0.255 atm

Temperature (˚C)	450	500	550	600	650	700
$ln\ k_{app,T}$	-4.66	-3.46	-2.76	-2.38	-1.99	-1.75
$ln\ k_T$	-3.27	-2.07	-1.37	-0.99	-0.61	-0.36

*k_T in $atm^{-1}min^{-1}$

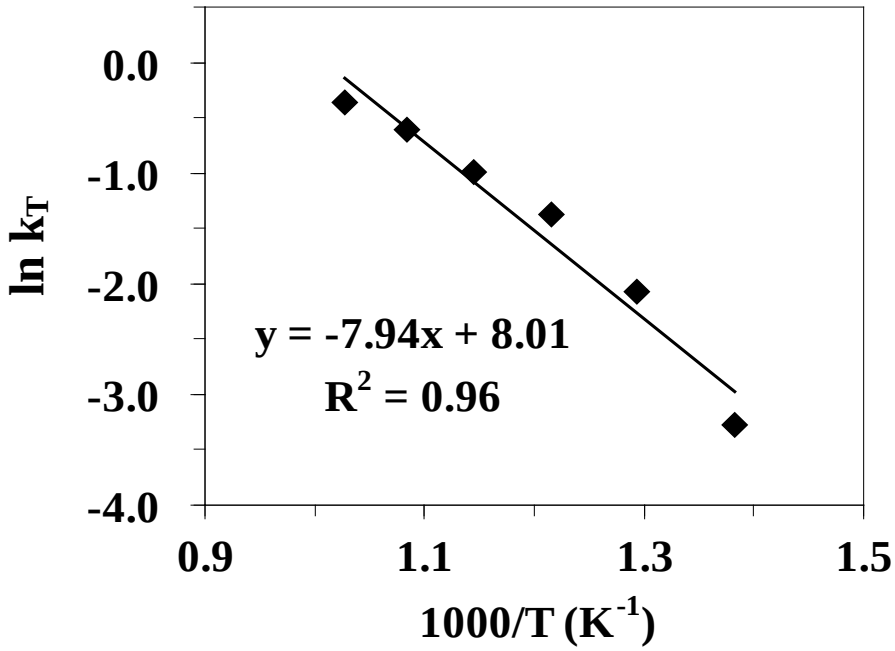

Figure 4-26 Arrhenius plot for k_T (in $atm^{-1}min^{-1}$)

Based on the above kinetics calculation and analysis, the final rate expression for this reduction process comes to be:

$$[-ln(1-X)]^{1/n} = k\,p_{co}{}^{m} \quad \text{---------- (4.6)}$$

with

$$k = k_o\,exp\,(-E_a/RT) \quad \text{---------- (4.7)}$$

where k_o is 3.01×10^3 $atm^{-1}min^{-1}$, and the units for p_{co} and t are atm and min, respectively. Also, n=1.26 and m=1.

As demonstrated in Figures 4-27 and 4-28, the reduction curves predicted by Equation 4.6 at different temperatures and CO contents adequately represent corresponding experimental data, especially at higher temperature and higher CO content.

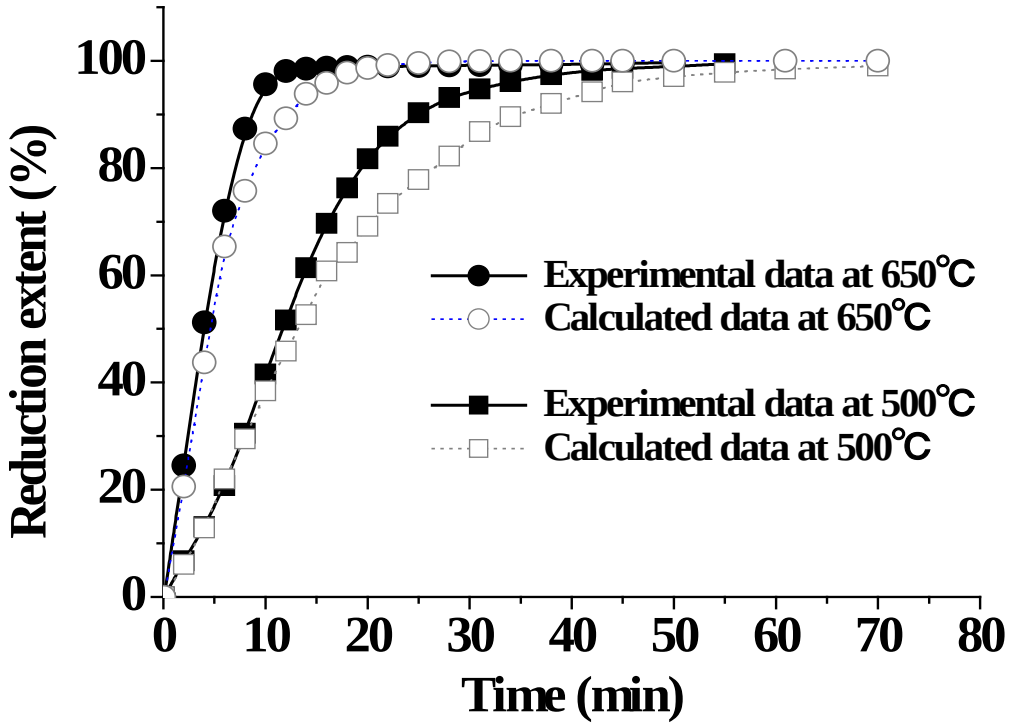

Figure 4-27 Comparison of experimental data and calculated date at different temperatures, CO/CO_2=30/70

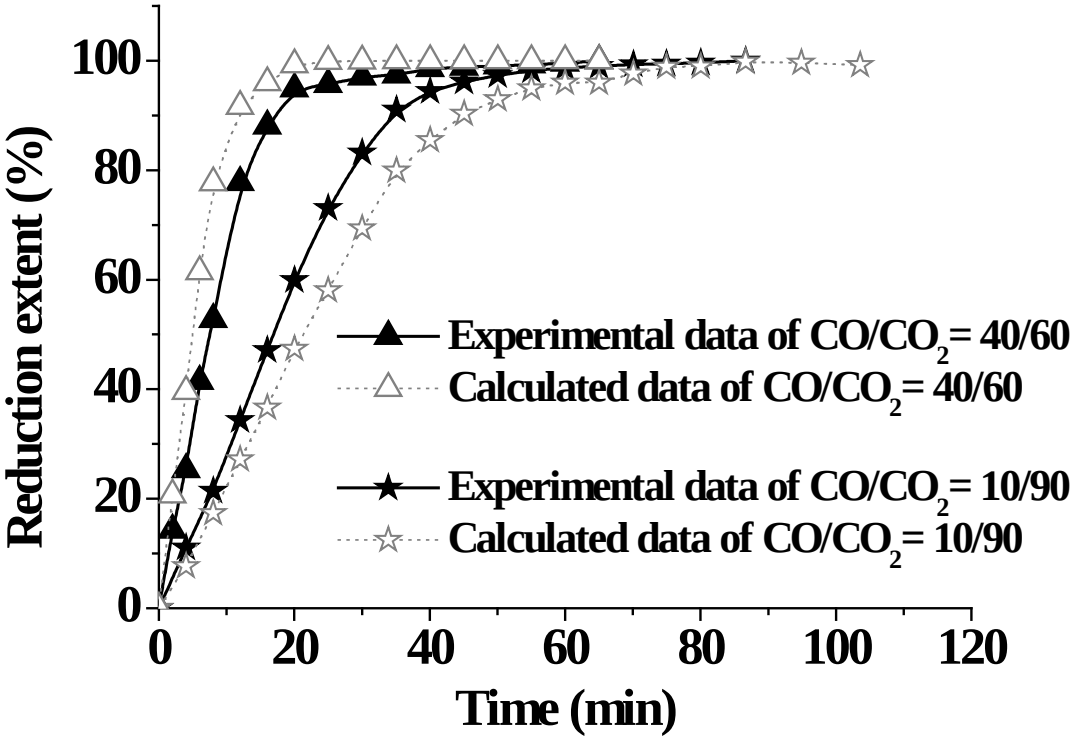

Figure 4-28 Comparison of experimental data and calculated data at different CO/CO_2 ratios, T= 600˚C

4.2.7 The effect of main impurities on the reduction process

The extent and rate of manganese ore reduction also depend on the ore composition. For calcinated "LP" ore, Fe_2O_3 and SiO_2 are the major impurities, and their effects were studied as follows.

4.2.7.1 Effect of Fe_2O_3 on the reduction of Mn_3O_4

To investigate the effect of Fe_2O_3 on the reduction of Mn_3O_4, several experiments were conducted at 600˚C, using a gas mixture of CO and CO_2 (CO/CO_2 = 30/70). Samples used in these tests consisted of Mn_3O_4 particles, which were prepared from 99.5% pure MnO_2, chemical reagent of Fe_2O_3 particles (99% purity), and the synthetic mixture of Fe_2O_3 and Mn_3O_4 in the same mass ratio as in the calcinated "LP" ore (Mn_3O_4/Fe_2O_3 = 4.2). All of the particles were in the size range of 105 ~ 150 μm. The reduction curves corresponding to different samples are shown in Figure 4-29.

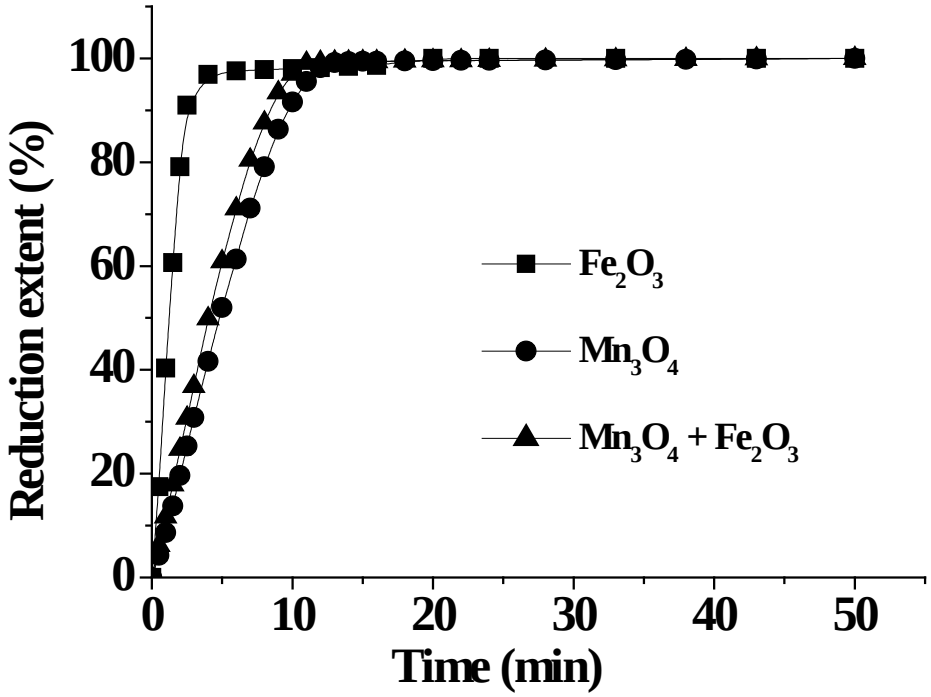

Figure 4-29 Reduction curves for different synthetic samples

It can be observed from Figure 4-29 that pure Fe_2O_3 particle is most readily reduced by CO than any other samples under the condition employed in this study. Besides, although the reduction rate of synthetic mixture is much slower than the reduction of pure Fe_2O_3, it is higher than the reduction of pure Mn_3O_4. This might be considered to be the catalytic effect of Fe_2O_3 on the reduction of Mn_3O_4, [27] but during this reduction progress, there is no distinct intermediate product of iron oxide and manganese oxide detected by XRD. Thus, it is more likely because the reduction rate of Fe_2O_3 by CO is much faster than that of Mn_3O_4, as a result, the overall reduction rate of their mixture is higher than that of Mn_3O_4. At the same time, the amount of Fe_2O_3 contained in the synthetic sample is too small for this effect to be appreciable. Therefore, the reduction curve of the mixture is very close to the curve of Mn_3O_4.

In addition, as shown in Figure 4-30, the reduction rate of calcinated "LP" ore is also close to that of synthetic mixture of Mn_3O_4 and Fe_2O_3. Meanwhile, it still could be observed from Figure 4-30 that the reduction rate of synthetic mixture of Mn_3O_4 and Fe_2O_3 is slightly faster than that of calcinated "LP" ore in the terminal stage of reduction. By comparing the composition of synthetic sample and that of calcinated "LP" Mn ore, we can find the major difference is that calcinated "LP" ore also contains considerable amount of silica besides Mn_3O_4 and Fe_2O_3. It is reported by Yastreboff [11] and Rankin[12] that the silica has a strong retarding effect on the carbothermic reduction of manganese ore. To study the reason accounting for the discrepancy in the reduction rate of synthetic mixture of Mn_3O_4 and Fe_2O_3 and that of calcinated "LP" Mn ore, it may also be necessary to further study the effect of silica on the reduction process.

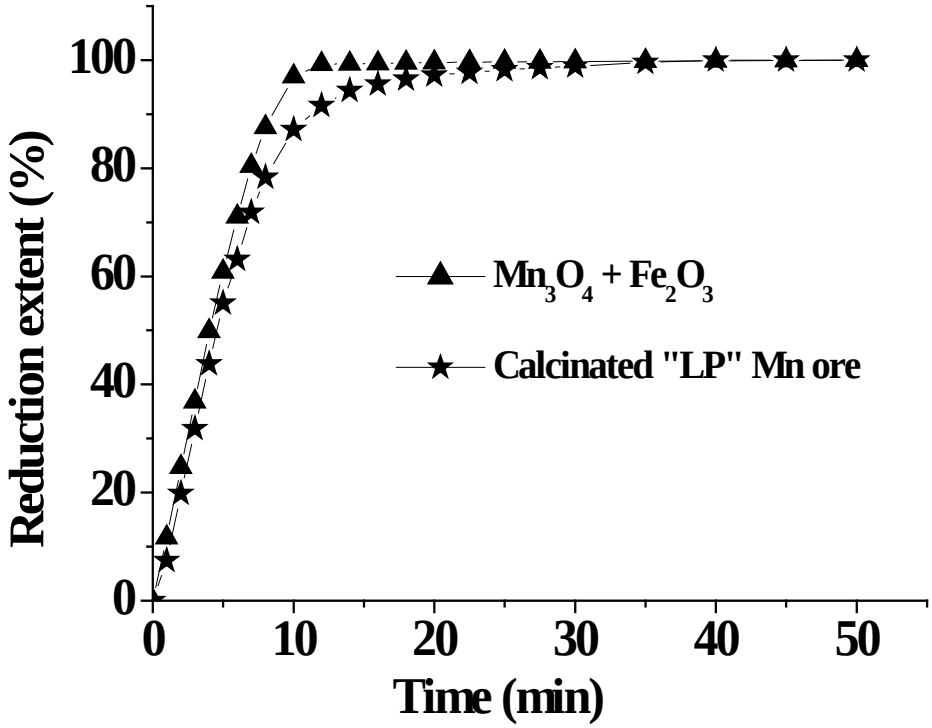

Figure 4-30 Reduction curves for synthetic mixture (Mn_3O_4 and Fe_2O_3) and calcinated "LP" ore

4.2.7.2 Efect of SiO_2 on the reduction process

The effect of SiO_2 on the reduction process was investigated by adding 99.8% pure SiO_2 to the synthetic mixture of Fe_2O_3 and Mn_3O_4. The Mn/Fe ratio of synthetic mixture is in the same ratio as in the calcinated "LP" ore, while the weight proportion of SiO_2 relative to the total weight of synthetic sample ranges from 10 to 30%. Reduction tests for these samples were conducted at 600˚C by a mixture gas of CO and CO_2 (CO/CO_2=30/70, the particle size of chemical reagents used in these tests was in the range of 105 ~ 150 μm.

The effect of SiO_2 on the reduction of Fe_2O_3 and Mn_3O_4 by CO is shown in Figure 4-31, from which it can be seen that the addition of SiO_2, under the experimental condition employed in this study, has no significant effect either on the reduction rate or

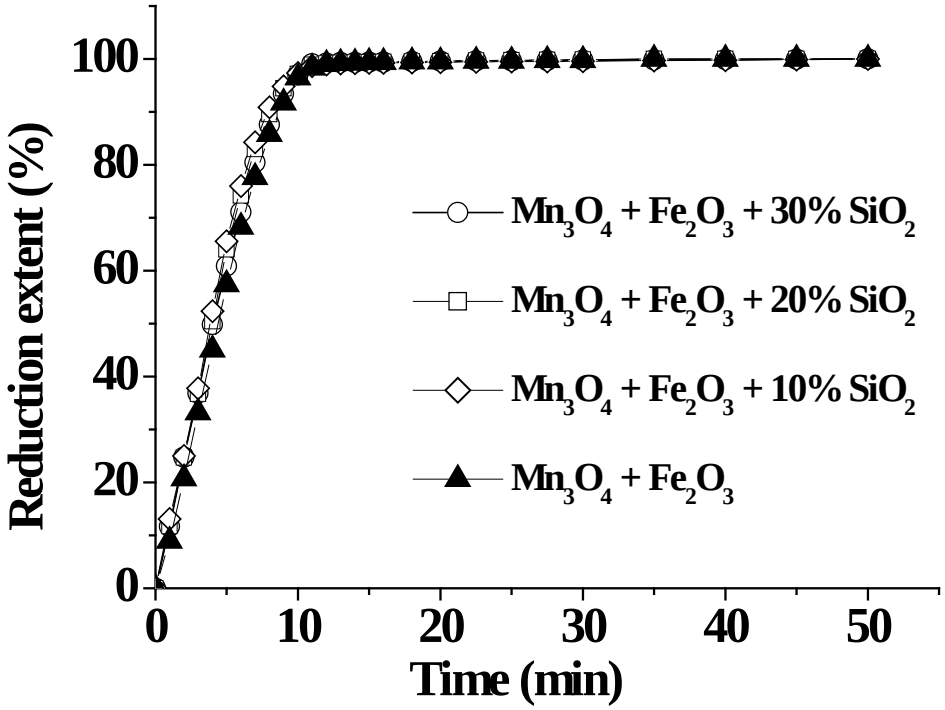

Figure 4-31 The effect of SiO_2 addition on the reduction of Mn_3O_4 and Fe_2O_3 by CO

on the reduction extent of the synthetic mixture of Fe_2O_3 and Mn_3O_4 at any weight ratio of SiO_2. This is different from the experimental test results obtained by Yastreboff [11] and Rankin, [12] who reported that silica had a retarding effect on the reduction of manganese ore due to the formation of silicate during the reduction process. The disagreement in test result is probably because the experimental temperature of this study (600˚C) is not high enough for SiO_2 to react with manganese oxide or iron oxide to form compound. Therefore, in this case, the discrepancy in the reduction rate of synthetic sample and that of calcinated "LP" ore is not due to the retarding effect of SiO_2.

The small discrepancy could most likely be explained by the lower reducibility of calcinated "LP" Mn ore, resulting from the difference in mineralogical conditions. For example, a small part of manganese or iron in the calcinated "LP" ore may exist as silicate compounds, although their corresponding peaks are not clearly detected in XRD

pattern because of the relatively small amount or maybe they are covered by the peaks of silica. The terminal reduction part of calcinated “LP” ore probably result from the reduction of these silicate compounds, which are not as reducible as oxides.

CHAPTER 5

CONCLUSIONS

Upgrading of ferruginous low-grade manganese ore used in this study, designated "LP", was successfully achieved through the prereduction by CO, followed by magnetic separation.

Under the optimum condition (particle size: <105 μm, reduction time: 25 minutes, temperature: 600˚C, CO content: 30 vol%) the Mn content in the "LP" ore increased from around 36% to more than 45%, and almost 50% of iron could be removed at a Mn loss around 5% after prereduction and magnetic separation. As a result, this can not only be beneficial regarding power consumption in the following process due to the enrichment of manganese, but also may lead to a large degree of freedom in mixing the charge for the production of ferromanganese, owing to a relative high Mn/Fe ratio achieved.

Meanwhile, it can also be noted from the test result of full factorial experiment that, within the range of various reduction parameters involved in this work, temperature has the strongest effect, followed by reduction time and CO content, and the significance of interaction effect is much smaller compared with the effect of each single reduction parameter.

From the kinetics study, it is found that the reduction rate is increased by an increase in the temperature and in CO content of reducing gas. The effect of particle size

on the reduction rate is not as notable as expected, because of the cracks formed during the reduction. Based on the experimental data as well as the physical condition of sample particles used in this work, the nucleation and growth rate equation best represent the data. The activation energy was determined to be 66 kJ/mol.

In addition, SiO_2 has no significant effect on the reduction of manganese oxides contained in the calcinated “LP” ore. The small difference in the reduction rate of synthetic sample and that of calcinated “LP” ore is most likely due to the difference in reducibility, resulting from the difference in mineralogical features.

. .

REFERENCES

[1] National Research Council Committee on Biologic Effects of Atmospheric Pollutants, *Manganese,* Washington, D.C.: National Academy of Sciences, ISBN 030902143X, 1973, p5.

[2] Hudnell K., Mergler D., Manganese: Essential Element and Neurotoxin, *Occupational Medicine Secrets*, Philadelphia: Haney & Belfus Inc., 1999, p81-84.

[3] U.S. Geological Survey, *Mineral Commodity Summaries*, 2004, p104-105.

[4] Sully A. H., *Manganese*, New York: Academic Press, 1955, p4.

[5] Harben P., Raleigh C., Harris J., *Manganese Uses & Markets*, New York: Industrial Minerals Information Ltd., 1998, p24.

[6] Elvers B., Hawkins S., Schulz G., *Ullmann's Encyclpedia of Industrial Chemistry*, Weinheim: VCH Verlagsgesellschaft mbH, 1990, p507.

[7] Hofmanne W., Vlajcic T., and Rath G.: Proc. Infacon 89, New Orleans, LA, *The Ferroalloys Association of the United States*, Arlington, VA, 1989, Vol. 1, p59-63.

[8] Ostrovski O., Webb, T. J. M., Reduction of Siliceous Manganese Ore by Graphite, *ISIJ International*, 35(11), 1995, p1331-1339.

[9] Eric R. H., Burucu E., The Mechanism and Kinetics of the Carbothermic Reduction of Mamatwan Ore Fines, *Minerals Engineering*, 5(7), 1992, p795-815.

[10] Hansen J. S., Tress J. E., Nafziger R.H., Carbothermic Reduction of US Ferruginous Manganese Resources, *JOM*, 45(4), 1993, p59-63.

[11] Yastreboff M., Ostrovski O., Ganguly S., Carbothermic Reduction of Manganese from Manganese Ore and Ferromanganese Slag, 8th International Ferroalloys Congress; Beijing; China, 1998, p263-270.

[12] Rankin W., Van Deventer J., The Kinetics of the Reduction of Manganese Oxide by Graphite, *JOM*, 80(7), 1980, p239-247.

[13] Antonov V. K. , Chufarov G. I., Trans.Inst. met. Akad. Nauk. U.S.S.R. Uralsk Filial, Vol 7, 1961, p101-105.

[14] Dewar K. , See J. B, Report No. 1968, National Institute of Metallurgy, The Influence of Carbonaceous Reducing Agents on the Rate of Reduction of Representative Manganese and Chromium Ores, Randburg, South Africa, 1978.

[15] Kor G. J. W., The Thermal Decomposition of Mn_2O_3 and the Reduction of Mn_3O_4 by C and CO, *Metallurgical Transactions B*, 9(3), 1978, p307-311.

[16] Kononov R., Ostrovski O., Ganguly S., Carbothermal Reduction of Manganese Oxide in Different Gas Atmosphere, *Metallurgical and Materials Transactions B*, 39(5), 2008, p662-668.

[17] Ding W.: Ph.D. Thesis, Equilibrium Relations in the Production of Manganese Alloys, University of Trondheim, Trondheim, Norway, 1993.

[18] Skjervheim T., Olsen S., The Rate and Mechanism for Reduction of Manganese Oxides from Silicate Slags. Paper in *INFACON 7*, ed. by Tuset J. K., H.Tveit, and I. G. Page (Proc. 7th Ferroalloys Congr., Trondheim, Norway, June 11-14, 1995), The Norwegian Ferro Alloy Research Organization (FFF) and SINTEF Materials Technology, Trondheim, Norway, 1995, p631-639.

[19] Yastreboff M., Ostrovski O., Ganguly S., Effect of Gas Composition on the Carbothermic Reduction of Manganese Oxide, *ISIJ International*, 43(2), 2003, p161-165.

[20] Anacleto N., Ostrovski O., Ganguly S., Reduction of Manganese Ores by Methane-containing Gas, *ISIJ International*, 44(10), 2004, p1615-1622.

[21] Kothari S. V., Nilkantha S. A., Process for the Reduction Roasting of Manganese Ores and a Device Thereof, US Patent: 5270022, 1993.

[22] Frenzel G., The Manganese Ore Minerals, In I.M. Varentsov and G. Grassely, Eds., *The Geology and Geochemistry of Manganese*, Vol. 2, 1980, p25.

[23] Gutzmer J., Beukes N. J., Kleyenstuber A. S. E., Burger A. M., Magnetic Hausmannite from Hydrothermally Altered Manganese Ore in the Paleoproterozoic Kalahari Manganese Deposit, Transvaal Supergroup, South Africa, *Mineralogical Magazine*, 109(1-2), 1995, p703–716.

[24] Sohn H. Y., Wadswarth M., *Rate Processes of Extractive Metallurgy*, New York: Plenum Press, 1979.

[25] Octave L., *Chemical Reaction Engineering*, Wiley Eastern Private Limited, New Delhi, 1969, p346.

[26] Avrami M., Kinetics of Phase Change II Transformation - Time Relations for Random Distribution of Nuclei, *The Journal of Chemical Physics*, 8(2), 1940, p212-225.

[27] Akdogan G., Eric R. H., Kinetics of the Solid-state Carbothermic Reduction of Wessel Manganese Ores, *Metallurgical and Marterials Transactions B*, 26(1), 1995, p13-24.